Hydraulic Criticality of the Exchange Flow through the Strait of Gibraltar

GIANMARIA SANNINO

Ocean Modelling Unit, ENEA, Rome, Italy

LAWRENCE PRATT

Woods Hole Oceanographic Institution, Woods Hole, Massachusetts

ADRIANA CARILLO

Ocean Modelling Unit, ENEA, Rome, Italy

ABSTRACT

The hydraulic state of the exchange circulation through the Strait of Gibraltar is defined using a recently developed critical condition that accounts for cross-channel variations in layer thickness and velocity, applied to the output of a high-resolution three-dimensional numerical model simulating the tidal exchange. The numerical model uses a coastal-following curvilinear orthogonal grid, which includes, in addition to the Strait of Gibraltar, the Gulf of Cadiz and the Alboran Sea. The model is forced at the open boundaries through the specification of the surface tidal elevation that is characterized by the two principal semidiurnal and two diurnal harmonics: M_2, S_2, O_1, and K_1. The simulation covers an entire tropical month.

The hydraulic analysis is carried out approximating the continuous vertical stratification first as a two-layer system and then as a three-layer system. In the latter, the transition zone, generated by entrainment and mixing between the Atlantic and Mediterranean flows, is considered as an active layer in the hydraulic model. As result of these vertical approximations, two different hydraulic states have been found; however, the simulated behavior of the flow only supports the hydraulic state predicted by the three-layer case. Thus, analyzing the results obtained by means of the three-layer hydraulic model, the authors have found that the flow in the strait reaches maximal exchange about 76% of the tropical monthlong period.

1. Introduction

The Strait of Gibraltar is a narrow and shallow channel 60 km long and 20 km wide, characterized by a complex system of contractions and sills (Fig. 1). In the eastern part of the strait a deep channel is present, called Tarifa Narrows (TN), characterized by a mean cross section of about 18 km and a depth of more than 800 m. To the west the bottom abruptly rises, reaching the minimum depth of the whole strait (284 m) at Punta Camarinal, determining the so-called Camarinal Sill (CS); then the bathymetry is characterized by the presence of a submarine ridge called Majuan Bank (MB in Fig. 1) dividing the cross section into two channels. The northern channel has a maximum depth of only 250 m, while the

southern channel has a maximum depth of 360 m that is actually a relative minimum depth for the main along-strait channel in the western part of the strait. This topographic point, called Espartel Sill (ES in Fig. 1), represents the last topographic constriction for the Mediterranean Outflow. Through this channel more than 80% of Mediterranean Water flows into the Gulf of Cadiz (Sanchez-Roman et al. 2009).

The mean circulation within the Strait of Gibraltar is described as an inverse estuarine circulation (Stommel and Farmer 1953), characterized by a two-way exchange, with an upper flow of fresh ($S_A \simeq 36.2$ psu) and warm Atlantic water spreading in the Mediterranean basin and a lower flow of cold and salty Mediterranean Water ($S_M \simeq 38.4$ psu) sinking in the North Atlantic down to a depth of ~1000 m where it becomes neutrally buoyant (Baringer and Price 1997; Ambar et al. 2002). While the excess evaporation over precipitation and river runoff that takes place in the Mediterranean Sea drives this

Corresponding author address: Gianmaria Sannino, via Anguillarese 301, Ocean Modelling Unit, ENEA, 00030 Rome, Italy.
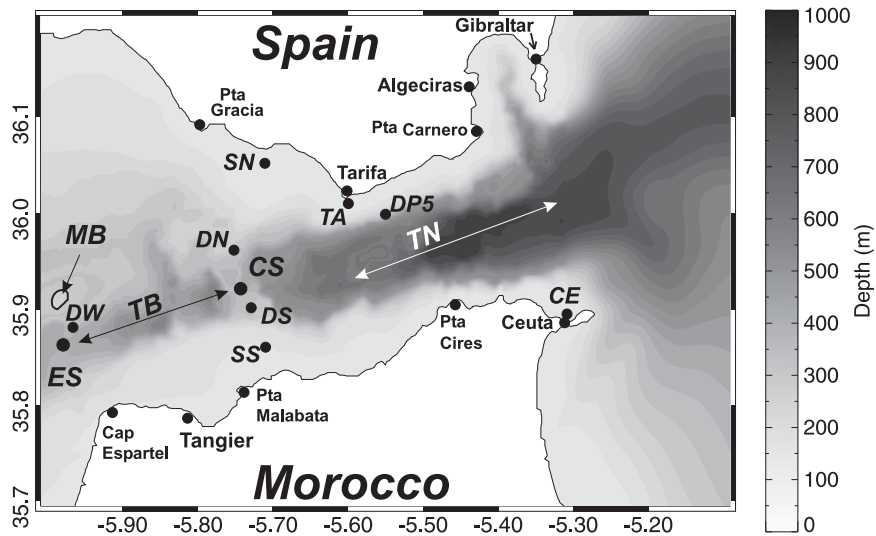E-mail: gianmaria.sannino@casaccia.enea.it

FIG. 1. Map of the Strait of Gibraltar showing the main topographic features—ES: Espartel Sill, TB: Tangier Basin, CS: Camarinal Sill, and TN: Tarifa Narrows. MB indicates the submarine ridge of Majuan Bank, located north of ES, dividing the cross section across ES in two channels. Other geographic locations referred to in the text are also shown.

mean circulation, its magnitude and hydrological properties strongly depend on the physical configuration of the strait (Bryden and Stommel 1984). In fact, it is well known that the Strait of Gibraltar is a place where the water exchange is subject to hydraulic control. However, a key issue that is still an open question regards the number and location of the hydraulic controls. These have a crucial role in forcing the strait dynamics toward one of the following two possible regimes: maximal and submaximal. If the exchange is subject to one hydraulic control in the western part of the strait, the regime is called submaximal while, if the flow exchange is also controlled in the eastern part of the strait along TN, the regime is called maximal. The two regimes have different implications for property fluxes, response time, and other physical characteristics of the coupled circulation in the strait and Mediterranean Sea. The maximal regime can be expected to have larger heat, salt, and mass fluxes and to respond more slowly to changes in stratification and thermohaline forcing within the Mediterranean Sea and the North Atlantic Ocean (Reid 1979).

Progress in understanding the hydraulic regime in the Strait of Gibraltar was made by Armi and Farmer (1988) and Farmer and Armi (1988, hereafter FA88) who analyzed data collected during the Gibraltar Experiment (Kinder and Bryden 1987). They approximated the vertical structure of the exchange flow as a two-layer system and showed the presence of four controls: two permanent and two episodic. The first permanent control was located west of ES, while the second was sited within TN, moving cyclically toward the east in accor-

dance with the eastward-traveling internal bore released by CS. The two episodic controls were located over the two sills Espartel and Camarinal. According to these findings the exchange flow was continuously in a maximal regime during the period of observation (April 1986).

Many papers have subsequently dealt with the applicability of the hydraulic theory to the exchange flow in the Strait of Gibraltar, focusing their analysis on the number and location of the hydraulic controls. Among others, see Bormans et al. (1986), Garrett et al. (1990), Bryden and Kinder (1991), García-Lafuente et al. (2000), and Send and Baschek (2001) for the experimental and analytical approach and Izquierdo et al. (2001) and Sannino et al. (2002) for numerical modeling studies. All of this work treats the exchange as a two-layer system. However, as demonstrated by Bray et al. (1995, hereinafter BR95), the two-way exchange is strongly affected by entrainment and mixing between the Atlantic and Mediterranean waters. Entrainment and mixing are sufficiently strong (Wesson and Gregg 1994) to lead to the formation of a thick interfacial layer where density and velocity change gradually in the vertical. The presence of this thick layer complicates the estimation of the hydraulic state by means of the two-layer hydraulic theory; in fact, depending on the way the currents and the thickness of both layers are defined, the values of the calculated hydraulic state may vary significantly (Send and Baschek 2001). Thus, in order to limit the arbitrariness in defining the interface, Sannino et al. (2007) proposed explicitly taking into account the three-layer

approximation introduced by BR95; in particular, they computed the hydraulic state applying the three-layer one-dimensional approximation derived by Smeed (2000). Results showed the presence of a periodic control over CS as for the two-layer case, but also a permanent supercritical region close to the north shore of TN near the Strait of Gibraltar.

It should be noted that all of the previous attempts to study the hydraulic criticality of the Strait of Gibraltar neglected the cross-strait variation of the layer thickness and velocity. However, even when idealized as a two- or three-layer system, the Gibraltar exchange flow is two-dimensional since cross-strait variations in velocity and layer thickness generally exist. The purpose of this paper is to assess the criticality of the exchange flow for both the two- and three-layer cases, including these cross-strait variations. To this end, the recent hydraulic criterion model developed by Pratt (2008) for an arbitrary number of layers, allowing for cross-channel variations in both thickness and velocity, has been adapted to the Strait of Gibraltar. The new criterion determines the hydraulic criticality of the flow as a whole across any section, and thereby removes any ambiguity that arises when the flow varies from being locally subcritical to supercritical across a section. The criterion has been used in synergy with a high-resolution three-dimensional numerical model designed to provide a very detailed description of the tidal exchange in the strait.

The present paper is organized as follows: the application of the hydraulic criterion to the strait is presented in section 2, while the numerical model used is described in section 3. Results obtained for the two- and three-layer system are shown in section 4, while conclusions are discussed in section 5.

2. The hydraulic criterion

a. Two-layer system

The hydraulic state of a steady, Boussinesq, two-layer flow with a rigid lid is determined by the value of the composite Froude number (Armi 1986)

$$G^2 = F_1^2 + F_2^2, \tag{1}$$

where $F_n = u_n/g'H_n$, u_n and H_n are the velocity and thickness of layer n, and g' is the reduced gravity. The flow is considered subcritical, critical, or supercritical, according to whether $G^2 < 1$, $G^2 = 1$, or $G^2 > 1$, respectively. A generalization to three-layer flow has been obtained by Smeed (2000). In both cases the flow is assumed to be one-dimensional so that cross-strait variations in layer thickness and velocity are not allowed.
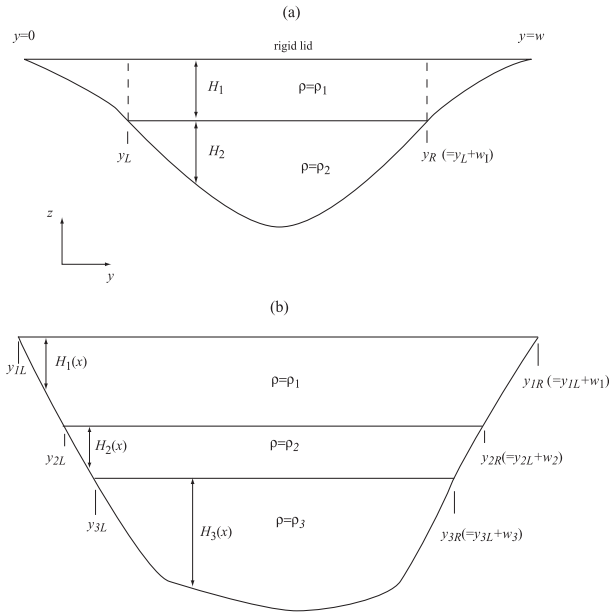

FIG. 2. Definition sketch for (a) two-layer and (b) three-layer flow.

In a two-layer system allowing cross-channel variations in layer velocities and thicknesses, the value of G^2 will vary across the channel and its value at any point is not a conclusive indicator of the hydraulic state (subcritical or supercritical) of the flow as a whole at that section. Rather, the hydraulic state depends on the propagation speed of long waves that exist across the entire section and satisfy bottom and sidewall boundary conditions. This complication can be dealt with when the layer thicknesses, but not the velocity, are allowed to vary across the strait. The procedure, described by Baines (1995), has been used to investigate the three-layer hydraulics of the Bab al Mandab (Pratt et al. 1999). When the layer depths and velocities vary, the criticality of the flow can be determined by a criterion developed by Pratt (2008). The procedure can be applied to an arbitrary number of layers, and we will do so for two- and three-layer representations of the flow through the Strait of Gibraltar. There are some caveats in the interpretation of the results, and these are described next.

For a two-layer system (Fig. 2a) the condition for critical flow is given by

$$G_w^2 = \frac{1}{w_I^{-1} \int_0^w (g'H_1/u_1^2)\,dy} + \frac{1}{w_I^{-1} \int_{yL}^{yR} (g'H_2/u_2^2)\,dy} = 1, \tag{2}$$

where w is the width of the surface and w_I the width of the interface. The generalized composite Froude number

defined in (2) reduces to the familiar G^2 when H_n and u_n are constants and $w = w_I$.

b. Three-layer system

For a three-layer system (Fig. 2b) the generalized critical condition is

$$\tilde{F}_1^2 + \left(\frac{1-r}{r} + \frac{w_3}{w_2}\right)\tilde{F}_2^2 + \tilde{F}_3^2 - \frac{w_3}{w_2}\tilde{F}_1^2\tilde{F}_2^2 - \tilde{F}_1^2\tilde{F}_3^2$$

$$- \frac{1-r}{r}\tilde{F}_2^2\tilde{F}_3^2 = 1, \qquad (3)$$

where

$$\tilde{F}_1^2 = \left(\frac{1}{w_2}\int_{y_1L}^{y_1R}\frac{g'_{21}H_1}{u_1^2}\,dy_1\right)^{-1},$$

$$\tilde{F}_2^2 = \left(\frac{1}{w_2}\int_{y_2L}^{y_2R}\frac{g'_{32}H_2}{u_2^2}\,dy_2\right)^{-1},$$

$$\tilde{F}_3^2 = \left(\frac{1}{w_3}\int_{y_3L}^{y_3R}\frac{g'_{32}H_3}{u_3^2}\,dy_3\right)^{-1}; \qquad (4)$$

$g'_{21} = g(\rho_2 - \rho_1)/\overline{\rho}$, $g'_{32} = g(\rho_3 - \rho_2)/\overline{\rho}$, $r = (\rho_2 - \rho_1)/(\rho_3 - \rho_1)$, and w_n is the width of the interface overlying layer n. Note that $\tilde{F}_1^2$, $\tilde{F}_2^2$ and $\tilde{F}_3^2$ can be interpreted as generalized versions of layer Froude numbers. It can be shown that (3) reduces to the condition derived by Smeed (2000) for the three-layer case when H_n and u_n are each uniform and $w_1 = w_2 = w_3$. It is tempting to think of the lhs of (3) as a composite Froude number and apply the same interpretations as for the two-layer composite Froude number G^2 (viz., that the flow is subcritical, critical, or supercritical according to $G^2 < 1$, $G^2 = 1$, or $G^2 > 1$). However, the left-hand side is clearly negative when all three individual Froude numbers are large and therefore a simple interpretation along the lines of the two-layer version is less obvious.

In a single-layer system with depth H and velocity u it is possible to decompose the phase speed into an advective part u and an intrinsic propagation part $\sqrt{gH}$, equal to the propagation speed in a resting fluid. In a multilayered system, this decomposition is possible only if the flow lacks shear, both horizontally and vertically. Thus, the layer Froude numbers in (4) are defined for convenience and cannot generally be thought of as ratios of intrinsic to advection speeds. To determine whether a particular state is subcritical, supercritical, or critical, it is helpful to rewrite (3) as

$$\frac{w_3}{w_2}\tilde{F}_2^2 = -\frac{(\tilde{F}_1^2 - 1)(\tilde{F}_3^2 - 1)}{(\tilde{F}_1^2 - 1) + \beta(\tilde{F}_3^2 - 1)}, \qquad (5)$$

where

$$\beta = \frac{w_2(1-r)}{w_3 r}.$$

Equation (5) defines a two-leafed surface in the space

$$\left(\tilde{F}_1^2, \frac{w_3}{w_2}\tilde{F}_2^2, \tilde{F}_3^2\right),$$

as shown in Fig. 3. The first leaf hovers slightly above the unit square ($0 \le \tilde{F}_1^2 \le 1$ and $0 \le \tilde{F}_3^2 \le 1$) of the horizontal plane [$(w_3/w_2)\tilde{F}_2^2 = 0$], while the second lies farther from the origin. We will denote by I, II, and III the three volumes between the two leafs. Flow states lying on either leaf are considered hydraulically critical in that at least one neutral long wave of the three-layer system has zero phase speed.

It remains to determine the hydraulic state of flows that exist in volumes I, II, and III. To this end, consider some horizontal [constant $(w_3/w_2)\tilde{F}_2^2$] slices through the volumes, as shown in Figs. 4a–c. Begin with the $(w_3/w_2)\tilde{F}_2^2$ plane, which is intersected by the critical surfaces along the lines $\tilde{F}_1^2 = 1$ and $\tilde{F}_3^2 = 1$, as shown in Fig. 4a. The projections of volumes I, II, and III are labeled, and it can be seen that II is divided into two subregions. At finite but small values of $(w_3/w_2)\tilde{F}_2^2$, specifically $(w_3/w_2)\tilde{F}_2^2 < (1+\beta)^{-1}$, region II is no longer divided (Fig. 4b). For $(w_3/w_2)\tilde{F}_2^2 > (1+\beta)^{-1}$, region I disappears altogether (Fig. 4c).

Now consider first the plane $(w_3/w_2)\tilde{F}_2^2 = 0$ in more detail. All flows lying therein have inactive middle layers, so the upper and lower layers are decoupled and act essentially as single layers. Were the layer depths and velocities uniform in y, the upper layer would support two long gravity waves with speeds $u_1 \pm (g'_{21}H_1)^{1/2}$, while the lower layer would have its own pair of waves with speeds of $u_3 \pm (g'_{31}H_3)^{1/2}$. In the unit square region (I) near the origin ($\tilde{F}_1^2 = u_1^2/g'_{12}H_1 < 1$, $\tilde{F}_3^2 = u_3^2/g'_{23}H_1 < 1$), the two upper-layer waves propagate in opposite directions, as do the two lower-layer waves. The flow is therefore hydraulically subcritical with respect to both upper-layer and lower-layer modes. It is easy to show that both waves belonging to the upper layer propagate in the same direction in region IIa, whereas the two lower-layer waves propagate in opposite directions. Region IIa therefore corresponds to supercritical flow with respect to just the upper-layer mode only. The reverse is true in region IIb. In region III the flow is supercritical with respect to both modes, meaning that all four waves propagate in the same direction, or that the two upper-layer waves propagate in one direction and the two lower-layer waves propagate in the other.
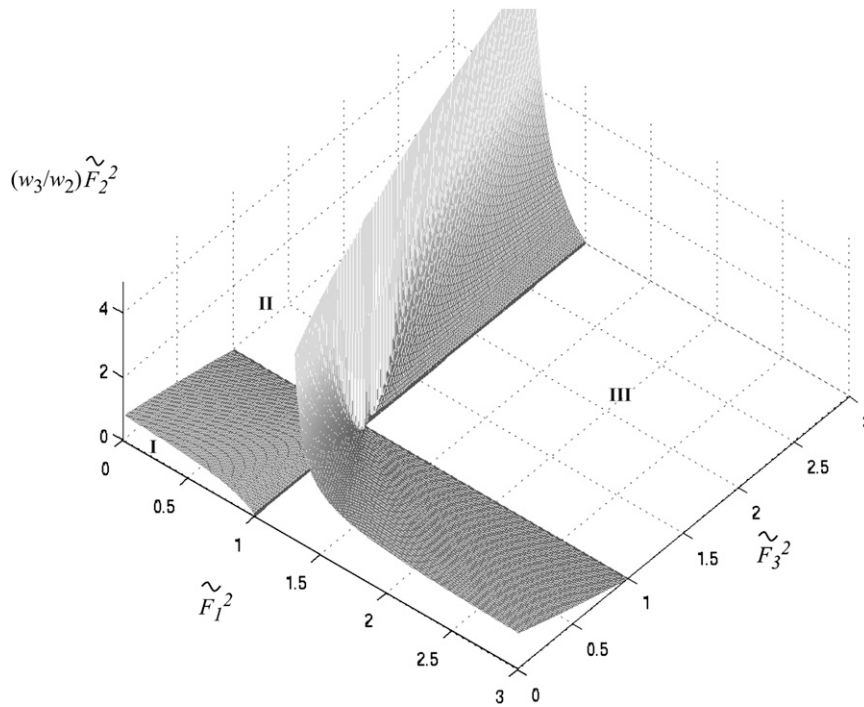
FIG. 3. Critical surface for $\beta = 0.25$.

It is now clear that volume I of Fig. 3 is bordered below by the subcritical region of the $(w_3/w_2)\tilde{F}_2^2$ plane just described. It is not difficult to show that this volume is also bordered on its sides (planes $\tilde{F}_1^2 = 0$ and $\tilde{F}_3^2 = 0$) by regions of flow that would be considered subcritical under traditional conditions (cross-strait independent velocities and layer thicknesses). We will therefore call states laying within volume I *provisionally subcritical*. The wave modes that arise in the interior of volume I generally cannot be decoupled into upper-layer and lower-layer modes as they were above, so it is not possible to refer to the upper or lower layer as being subcritical. Instead, one must speak of subcriticality with respect to the two wave modes, which are related to the first and second baroclinic modes of a continuously stratified flow. Similarly, flow states laying within volume II will be categorized as provisionally supercritical with respect to one mode. Again, this volume is bordered by regions that, under traditional conditions, would be supercritical with respect to one of the internal modes, but not the other. Volume III is considered provisionally supercritical with respect to both modes. Classification of the flow in any region is further complicated by the presence of lateral shear, which may give rise to wave modes not present in the traditional three-layer system. Also, imaginary phase speeds (long-wave instability) are common within both of the supercritical regions, even in the traditional case. In interpreting the critical con-

ditions (2) or (3), or Figs. 3 and 4, it should be kept in mind that the long-wave speeds depend on the shear between and across the layers, and cannot generally be expressed as the sum of a current speed and a resting propagation speed. Thus, the Froude numbers $\tilde{F}_1$, $\tilde{F}_2$, and $\tilde{F}_3$ are defined for convenience and do not have a simple meaning in terms of propagation speeds or their components.

To locate the volume that a particular flow state lies within, first calculate the values of $\tilde{F}_1^2$, $(w_3/w_2)\tilde{F}_2^2$, and $\tilde{F}_3^2$. Let Z represent $(w_3/w_2)\tilde{F}_2^2$, and let $Z_c(\tilde{F}_1^2, \tilde{F}_3^2)$ represent the critical surface defined by (5). If

$$\tilde{F}_3^2 < \frac{1+\beta}{\beta} - \frac{\tilde{F}_1^2}{\beta}, \qquad (6)$$

then $Z < Z_c$ means that the flow is provisionally subcritical, while $Z > Z_c$ means that the flow is provisionally supercritical with respect to just one mode; whereas, if

$$\tilde{F}_3^2 > \frac{1+\beta}{\beta} - \frac{\tilde{F}_1^2}{\beta}, \qquad (7)$$

then $Z < Z_c$ means that the flow is provisionally supercritical with respect to one mode, while $Z > Z_c$ means that the flow is provisionally supercritical with respect to both modes (note that Z_c may be <0).
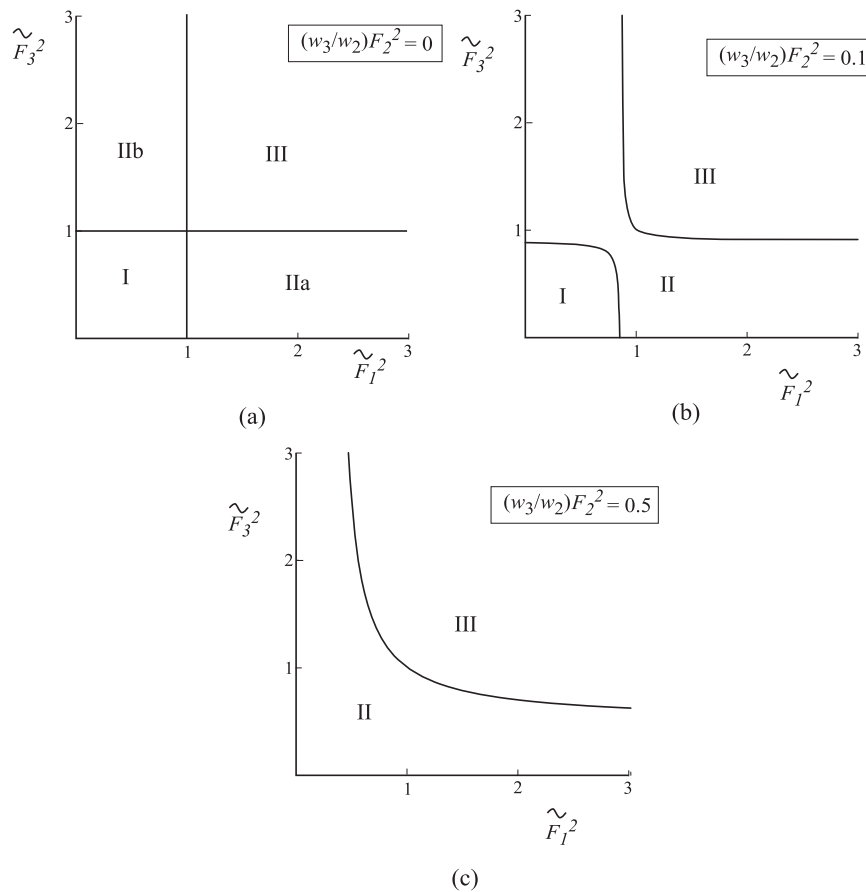
FIG. 4. Slices of constant $(w_3/w_2)\tilde{F}_2^2$ for $\beta = 0.25$.

One result that may be relevant to the Strait of Gibraltar is that if the intermediate layer experiences some interval across the strait over which the velocity u_2 is very small, then $(w_3/w_2)\tilde{F}_2^2$ will be quite small and the upper and lower layers become decoupled. Thus, decoupling of the upper and lower layer does not require that u_2 be zero across the entire strait, at least not in terms of hydraulic control of the flow.

c. Further remarks on the behavior of long waves and stability

This section attempts to develop further insight into the meaning of volumes I, II, and III of Fig. 3. An uninterested reader may skip this discussion and proceed to section 3. We examine the wave speeds themselves and, for simplicity, consider the traditional setting in which the channel cross section is rectangular ($w_1 = w_2 = w_3$) and u_i are independent of y. Under these conditions $\tilde{F}_i$ reduces to the ordinary Froude number for each layer. The long-wave speeds can be calculated from Eq. (2.7) of Pratt et al. (1999) and can be shown to depend on the three Froude numbers as well as the value of

r and the dimensionless depth ratios $d_1 = H_1/H$ and $d_2 = H_2/H$, where $H = H_1 + H_2 + H_3$.

As a first example, consider the variations of phase speeds along a line defined by $\tilde{F}_1^2 = \tilde{F}_2^2 = \tilde{F}_3^2$ in the space of Fig. 3. One can begin at the origin and follow this line outward as it cuts through the two surfaces separating volumes I, II, and III. The phase speeds depend on the signs of $\tilde{F}_i$, which we take to be positive, so the flow is unidirectional. We also assume that $r = 0.5$ and that the layer depths are equal ($d_1 = d_2 = 1/3$) so that the layer velocities are equal and there is no interfacial shear. The results are plotted in Fig. 5a as a function of $\tilde{F}_1$. The system contains two pairs of internal long waves, and we denote their nondimensional speeds (scaled by $g_{23}'H$) $c_1^\pm$ and $c_2^\pm$. At $\tilde{F}_1 = 0$ the background state is quiescent and each pair of speeds is evenly distributed around zero. Here $c_1^\pm$ are easily identifiable as the speeds of the first baroclinic mode. Their magnitude exceeds that of the speeds $c_2^\pm$ of the second baroclinic mode. As $\tilde{F}_1$ increases, the flow moves as a slab with an increasing velocity and the modes are advected in the same direction. The system first becomes supercritical with respect
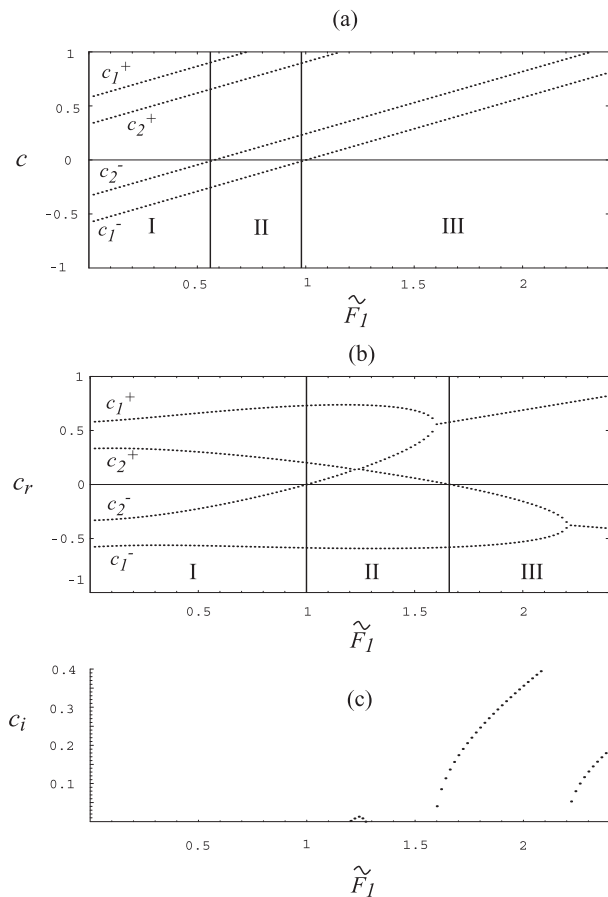
(a)

(b)

(c)

FIG. 5. Phase speeds for the four long waves of a traditional three-layer system with no cross-channel variations in layer thicknesses or velocities. (a) The phase speeds as functions of $\tilde{F}_1$ for the unidirectional slab flow $\tilde{F}_1^2 = \tilde{F}_2^2 = \tilde{F}_3^2$, $d_1 = d_2 = \frac{1}{3}$ and $r = 0.5$. (b) Real and (c) imaginary parts of the waves speeds are plotted for the same r and d_n, but under the exchange flow conditions $\tilde{F}_3 = -0.6\tilde{F}_1$ and $\tilde{F}_2 = 0.1\tilde{F}_1$.

to the second mode near $\tilde{F}_1 = 0.56$, and with respect to both modes near $\tilde{F}_1 = 1$. The vertical lines that mark these transitions coincide with the boundaries separating volumes I, II, and III.

An example that is more realistic for exchange flow has the same settings above but with $\tilde{F}_3 = -0.6\tilde{F}_1$ and $\tilde{F}_2 = 0.1\tilde{F}_1$. The presence of shear between the layers makes long-wave instability possible and the real and imaginary parts of the wave speeds are shown separately in Figs. 5b and 5c. Near $\tilde{F}_1 = 0$ the modes are stable and separated into two pairs. As $\tilde{F}_1$ increases, c_2^- undergoes a zero crossing and the subcritical flow becomes supercritical with respect to the second internal mode. At a slightly larger value of $\tilde{F}_1$, c_2^- and c_2^+ briefly merge, producing a small band of long-wave instability. The positive imaginary part of c_2 is plotted in Fig. 5c, and the instability appears as a small mound of positive values
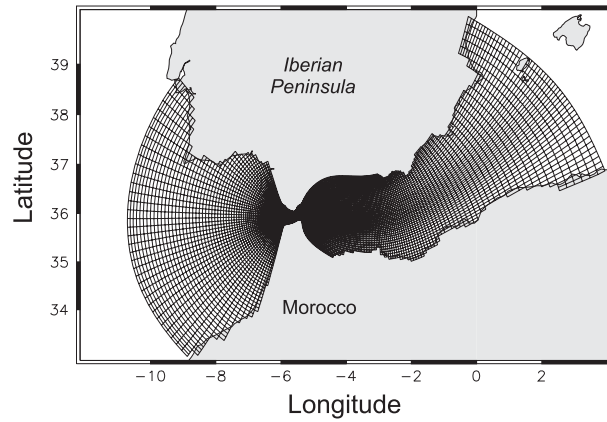

FIG. 6. Horizontal model grid.

about $\tilde{F}_1 = 1.25$. At slightly larger $\tilde{F}_1$ the two modes separate and the flow once again becomes stable and supercritical with respect to one mode. However, two other waves merge near $\tilde{F}_1 = 1.6$, and the flow again becomes unstable. At slightly larger $\tilde{F}_1$, one of the neutral modes undergoes a zero crossing and this marks the transition from region II to region III. In the latter, there is one unstable mode pair, each member having the same real speed (c_r) but with equal and opposite imaginary parts, and one pair of neutral waves with negative phase speeds. This pair later merges and becomes unstable as well. As the reader can see, the journey from region I to III is complex, with mergers between different wave components and resulting instabilities. At the boundaries between the regions, at least one neutrally stable, stationary long wave exists, but the other waves may have imaginary speeds.

3. Numerical model description

The numerical model used for this study is the three-dimensional σ-coordinate Princeton Ocean Model (POM) designed in the late 1970s by Blumberg and Mellor (1987) to study both coastal and open ocean circulation. The model uses a curvilinear orthogonal grid covering the region between the Gulf of Cadiz and the Alboran Sea (Fig. 6). The grid has a nonuniform horizontal spacing; horizontal resolution is higher in the strait, where it is around 300 m, with respect to the eastern (western) ends where it reaches 10–20 km (8–15 km). The portion of the horizontal grid representing the strait is rotated anticlockwise ~17° so that the along-strait velocity is quite well represented by the model u component (Fig. 7). The vertical grid is made of 32 sigma levels, logarithmically distributed at the surface and the bottom and uniformly distributed in the rest of the water column. Model topography has been obtained by merging the 2-min
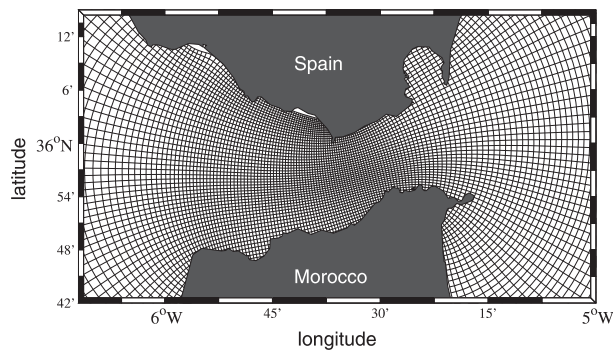
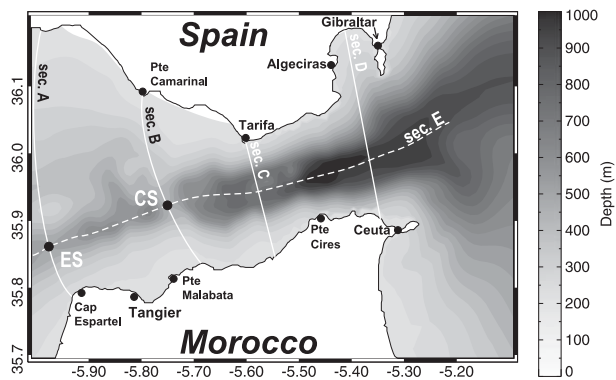FIG. 7. Horizontal model grid for the region of the strait.

FIG. 8. Model bathymetry for the region of the strait. Gray levels indicate the water depth. The point ES and CS represent the position for Espartel Sill and Camarinal Sill, respectively. White lines indicate sections used to present model results.

Gridded Global Relief Data (ETOPO2) bathymetry (U.S. Department of Commerce and NOAA/NGDC 2001) with the very high resolution digitalized bathymetry provided by the Physical Oceanographic Group of the University of Malaga. To reduce the well-known pressure gradient error produced by sigma coordinates in regions of steep topography (Haney 1991), a smoothing was applied in order to reach values of $\delta H/H < 0.2$, where H is the model depth, as suggested by Mellor et al. (1994). The resulting model topography in the region of the strait is shown in Fig. 8. Two open boundaries are defined at the eastern and western ends of the computational domain; here, an Orlanski radiation condition (Orlanski 1976) is used for the depth-dependent velocity, while a forced Orlanski radiation condition (Bills and Noye 1987) is used for the surface elevation and a zero gradient condition for the depth-integrated velocity. Boundary conditions for both temperature and salinity are specified by using an upwind advection scheme that allows advection of temperature and salinity into the model domain under inflow conditions. Normal velocities are set to zero along coast boundaries, while at the bottom an adiabatic boundary condition is applied to temperature and salinity; finally, a quadratic bottom friction with a prescribed drag coefficient is applied to the momentum flux. The Smolarkiewicz upstream-corrected advection scheme for tracers (Smolarkiewicz 1984), as implemented by Sannino et al. (2002), was used in the present study. The model resolves the vertical subgrid-scale turbulence by prognostic equations for the turbulent velocity and length scale (Mellor and Yamada 1982); thus, there is no need for specific parameterizations of entrainment, as recently demonstrated by Ezer (2005). This feature makes our model capable of taking into account the effect of entrainment and mixing between Atlantic and Mediterranean waters. The model starts from rest and is forced at the open boundaries through the specification of the surface tidal elevation characterized by the principal two semidiurnal and two diurnal harmonics: M_2,

S_2, O_1, and K_1. Amplitude and phase of these harmonics have been computed via the OTIS package (Egbert and Erofeeva 2002). Finally, the initial conditions in terms of salinity and temperature have been taken from the Mediterranean Data Archaeology and Rescue (MEDAR)/ Mediterranean Hydrological Atlas (MEDATLASII) climatologic Mediterranean and Black Sea Database (MEDAR Group 2002) for the month of April. The present model can be considered as an improved version of the model implemented by Sannino et al. (2007) as it is characterized by a better resolved bathymetry and more realistic initial and boundary conditions.

The model was initially run for 240 days without tidal forcing in order to achieve a steady two-way exchange system. Then, the model simulation was extended for another 7 days forced by tidal components in order to achieve a stable time periodic solution. Finally, the model was run for a further tropical month (27.321 days) that represents our main experiment. The term "time averaged" that will be used in the following refers to the average over this tropical month period. Spring tide corresponds to day 21 of the simulation; neap tide to day 27.

Model validation

A complete validation analysis of the numerical model has been performed by Sanchez-Roman et al. (2009). In their work they compared the predicted and observed amplitude and phase of the diurnal and semi-diurnal tidal components of the along-strait velocity field; in particular, they first collected data for the month of April from different observed datasets along the strait and from the model simulation for the same locations, and then applied to them the classical Foreman vectorial harmonic analysis (Foreman 1978; Pawlowicz et al. 2002). The results obtained were considered satisfactory,

TABLE 1. Comparison between observed and predicted amplitudes A and phases P of the M_2 tidal elevation.

Location	Lat	Lon	Observed M_2		Predicted M_2		Predicted − observed		
			A (cm)	P (°)	A (cm)	P (°)	A (cm)	A (%)	P (°)
Tsimplis et al. (1995)									
Gibraltar	36°08′	05°21′	29.8	46.0	29.5	46.0	−0.3	1.0	+0.0*
García-Lafuente (1986)									
Punta Gracia	36°05.4′	05°48.6′	64.9 ± 0.2	49.0 ± 0.5	67.6	53.8	+2.7	4.1	+4.5
Tarifa	36°00.2′	05°36.4′	41.5 ± 0.2	57.0 ± 0.5	43.5	49.7	+2.0	4.8	−7.3
Punta Cires	35°54.7′	05°28.8′	36.4 ± 0.2	46.5 ± 0.5	35.0	54.9	−1.4	3.8	+8.4
Punta Carnero	36°04.3′	05°25.7′	31.1 ± 0.2	47.5 ± 0.5	30.8	47.4	−0.3	0.9	−0.1
Candela et al. (1990)									
DN	35°58′	05°46′	60.1	51.8	58.2	57.8	−1.9	3.1	+6.0
DS	35°54′	05°44′	54.0	61.8	54.1	64.1	+0.1	0.2	+2.3
SN	36°03′	05°43′	52.3	47.6	52.3	52.9	0.0	0.0	+5.3
SS	35°50′	05°43′	57.1	66.8	56.8	67.4	−0.3	0.5	+0.6
DW	35°53′	05°58′	78.5	56.1	76.6	62.7	−1.9	2.4	+6.6
TA	36°01′	05°36′	41.2	41.2	43.5	49.7	+2.3	5.5	+8.5
AL	36°08′	05°26′	31.0	48.0	30.0	49.7	−1.0	3.2	+1.7
CE	35°53′	05°18′	29.7	50.3	29.5	51.5	−0.2	0.6	+1.2
DP5	36°00′	05°34′	44.4	47.6	42.1	47.6	−2.3	5.1	+0.0

* Calibration.

with differences limited in most of the strait to less than 10 cm s^{-1} in amplitude and 20° in phase.

Good agreement between observed and model data also has been found for the surface elevation. In Tables 1 and 2 the observed amplitudes (A) and phases (P) of the two semidiurnal tidal components [that represent more than 80% of the total tidal signal according to Candela et al. (1990)] of the surface elevation are compared with the simulated amplitudes (A) and phases (P) of the same components. Here one can see that the

maximum differences do not exceed 3.6 cm in amplitude (with a maximum error that however does not exceed 18%) and 11° in phase.

The model is also able to reproduce the generation and subsequent propagation of the internal bores with characteristics similar to those described by FA88 (see Fig. 9). About 1 h before high tide at Tarifa the internal bore is released from CS (Fig. 9a) and starts to travel eastward. The bore is released when the upper layer starts to move eastward, while the lower layer continues

TABLE 2. Comparison between observed and predicted amplitudes A and phases P of the S_2 tidal elevation.

| Location	Lat	Lon	Observed S_2		Predicted S_2		Predicted − observed		
			A (cm)	P (°)	A (cm)	P (°)	A (cm)	A (%)	P (°)
Tsimplis et al. (1995)									
Gibraltar	36°08′	05°21′	10.7	72.0	11.6	72.0	+0.9	8.4	+0.0*
García-Lafuente (1986)									
Punta Gracia	36°05.4′	05°48.6′	22.3 ± 0.2	74.0 ± 1.0	25.9	77.6	+3.6	16.1	+3.6
Tarifa	36°00.2′	05°36.4′	14.2 ± 0.2	85.0 ± 1.5	16.8	73.9	+2.6	18.3	−11.1
Punta Cires	35°54.7′	05°28.8′	14.1 ± 0.2	74.0 ± 1.	14.5	81.2	+0.4	2.8	+7.2
Punta Carnero	36°04.3′	05°25.7′	11.5 ± 0.2	71.0 ± 1.0	12.1	72.0	+0.6	5.2	+1.0
Candela et al. (1990)									
DN	35°58′	05°46′	22.5	73.8	22.4	81.4	−0.1	0.4	+7.6
DS	35°54′	05°44′	21.1	83.3	20.7	88.2	−0.4	1.9	+4.9
SN	36°03′	05°43′	18.5	73.4	20.6	76.3	+2.1	11.3	+2.9
SS	35°50′	05°43′	20.6	92.3	21.9	91.0	+1.3	6.3	−1.3
DW	35°53′	05°58′	29.0	82.2	29.2	85.4	+0.2	0.7	+3.2
TA	36°01′	05°36′	14.7	67.9	17.3	72.8	+2.6	17.7	+4.9
AL	36°08′	05°26′	11.1	73.9	11.7	75.0	+0.6	5.4	+1.1
CE	35°53′	05°18′	11.4	75.6	11.8	78.1	+0.4	3.5	+2.5
DP5	36°00′	05°34′	16.1	73.9	16.2	72.6	+0.1	0.6	−1.3

* Calibration.
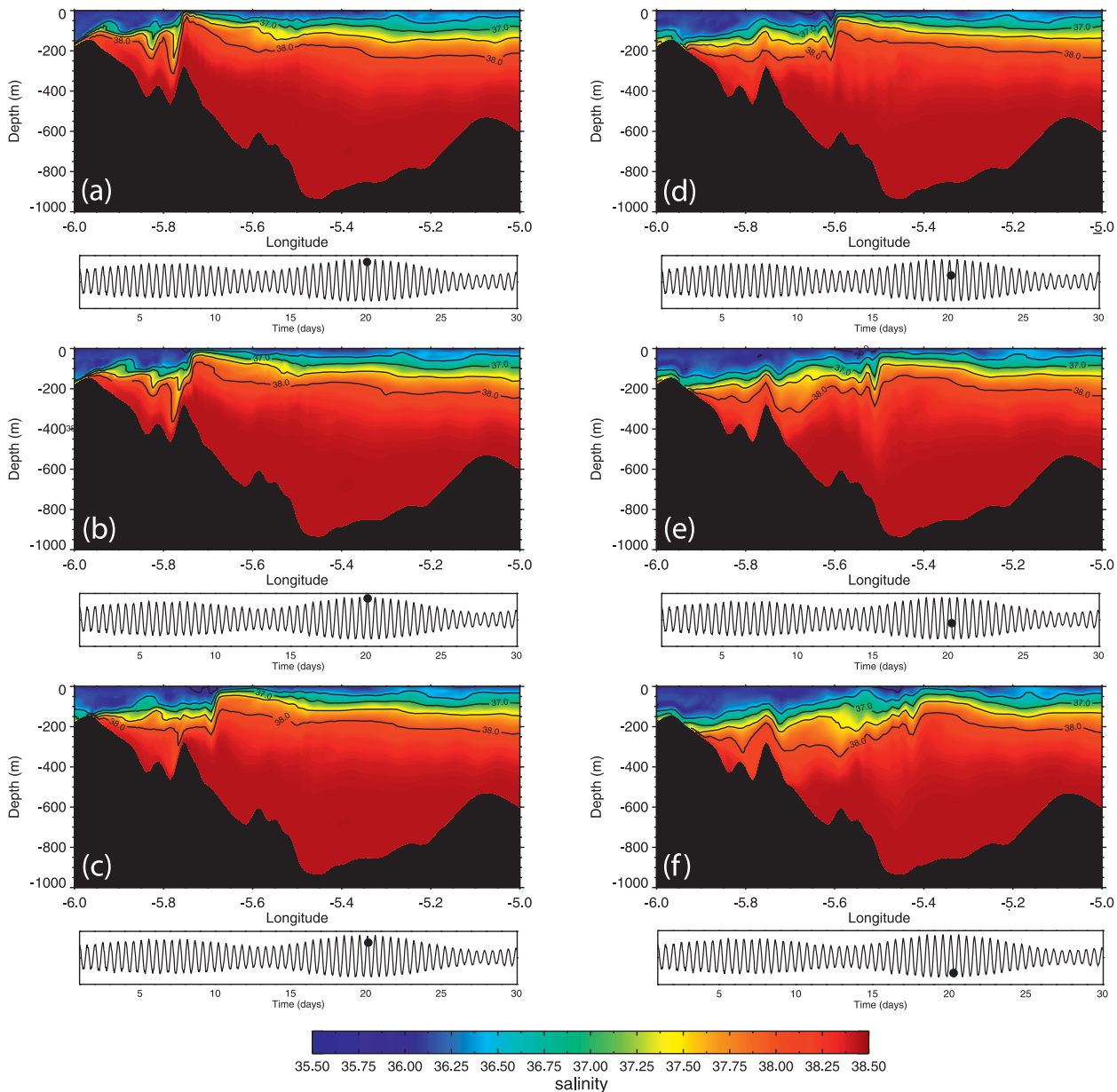
FIG. 9. (a)–(f) Evolution of salinity pertubations during spring tide. Contours are shown with an interval of 0.5 psu. The snapshots are plotted at an interval of 1 h. The time moments are referred to the surface elevation at Tarifa.

to move westward. Its initial length scale, in the along-strait direction, is about 3 km and its travel times from CS to Tarifa, Punta Cires, and Gibraltar sections are 2, 4, and 6 h, corresponding to a speed of about 1.7 m s^{-1} between Camarinal Sill and Tarifa, 2.5 m s^{-1} between Tarifa and Punta Cires, and 1.5 m s^{-1} between Punta Cires and Gibraltar sections. The amplitude of the eastward propagating bore decreases progressively from about 100 m on the western edge of CS to about 50 m at the Gibraltar section. Initially the bore is characterized by two large and steep internal waves that during the

eastward propagation disintegrate, at the exit of the strait, into dispersive wave trains.

However, what is observed in the Strait of Gibraltar is that the bore, at the eastern exit of the strait, disintegrates into rank-ordered sequences of internal solitary waves followed by a dispersive wave (Brandt et al. 1996). The model is not able to reproduce these internal solitary waves as nonhydrostatic effects are neglected. However, given that most of the principal bore characteristics are well simulated by the model both at CS and along TN, it can be considered as a suitable tool for

studying the criticality of the flow exchange in the Strait of Gibraltar.

4. Results

In this section output obtained from running the main numerical experiment will be analyzed on the basis of the hydraulic condition described in section 2. The analysis will be conducted first for the two-layer and subsequently for the three-layer case. Note that the cross-strait layer velocity u_n and the layer density ρ_n used in the following hydraulic analysis are computed as

$$u_n(x, y, t) = \int_{dw_n(x,y,t)}^{up_n(x,y,t)} u(x, y, z, t)\, dz, \qquad (8)$$

$$\rho_n(x, t) = \int_{yS_n(x)}^{yN_n(x)} \int_{dw_n(x,y,t)}^{up_n(x,y,t)} \rho(x, y, z, t)\, dz\, dy, \qquad (9)$$

where up_n and dw_n are the instantaneous depths of the upper and lower bounds of the nth layer and yS_n and yN_n represent the southern and northern limit of the cross section x and nth layer.

Owing to the bathymetric structure of the western part of the strait, the hydraulic analysis in that region will be restricted to the southern channel only.

a. Two-layer approximation

To identify regions where the flow is hydraulically controlled in the two-layer approximation, the instantaneous generalized composite Froude number (G_w^2) is evaluated following Eq. (2) and considering ρ_1 and ρ_2 as the mean density of the upper and lower layer, respectively. To carry out the analysis it is necessary first to define an interface between Mediterranean and Atlantic waters. The method used consists in defining the interface as the tropical month-averaged salinity surface corresponding to the zero tropical month-averaged velocity field. The internal salinity surface obtained is shown in Fig. 10. As expected, the salinity increases from west to east changing from about 37.25 psu at CS up to about 38.1 psu at the east entrance of the strait. The value 37.25 psu is in agreement with those used by Bryden et al. (1994) and Candela et al. (1989) to compute the volume transport across a section passing through CS, while the value 38.1 psu is the same as adopted by Candela et al. (1989) and Baschek et al. (2001) to compute the transport through a cross section at the eastern end of the strait. Using this material interface the instantaneous generalized composite Froude number (G_w^2) has been computed. Looking at Fig. 11a, which shows the frequency of occurrence of supercritical composite Froude number over the tropical month pe-

Salinity Interface (psu)

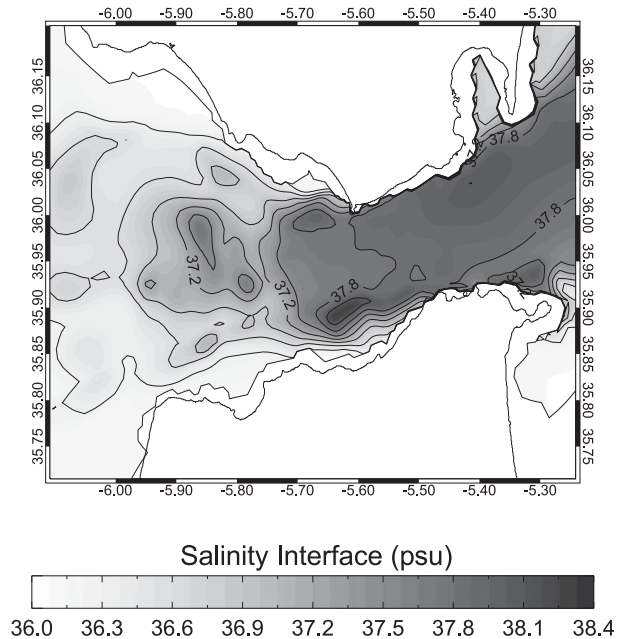36.0   36.3   36.6   36.9   37.2   37.5   37.8   38.1   38.4

FIG. 10. Time-averaged interfacial-layer salinity for the two-layer approximation.

riod, it appears evident that the frequency is low in TN, while higher values are reached in the region of CS and ES; in particular, at CS the frequency is 50% while west of ES it is about 20%. As expected the critical condition in TN is primarily due to the upper-layer flow ($\tilde{F}_1^2 \gg \tilde{F}_2^2$), while at ES and CS it is primarily due to the lower-layer flow.

While the previous description is useful in identifying the regions within the strait where the flow becomes supercritical, a complete understanding of the hydraulic regimes, in terms of maximal or submaximal exchange, can be achieved only by exploring the simultaneous presence of supercritical flow regions through the strait. This is done in Fig. 12, where, in the light of the previous findings, the analysis is restricted over the two sills of CS and ES and the region of TN. The bars indicate the presence of supercritical flow in those regions. It can be shown that the lower-layer Froude number is dominant at ES and CS, the upper layer being relatively inactive, while the upper layer is dominant at TN. At CS the flow is supercritical two times per semidiurnal period except during neap tide when it becomes supercritical only once per diurnal period. In general, the flow reaches a supercritical state during high water in Tarifa, and then the control is lost and recovered again during the subsequent rising tidal phase. Criticality of the flow at ES shows a quite different behavior during spring and neap tide. During spring tide (from day 7 to 10 and from day 16 to 23) the flow appears to be supercritical for every
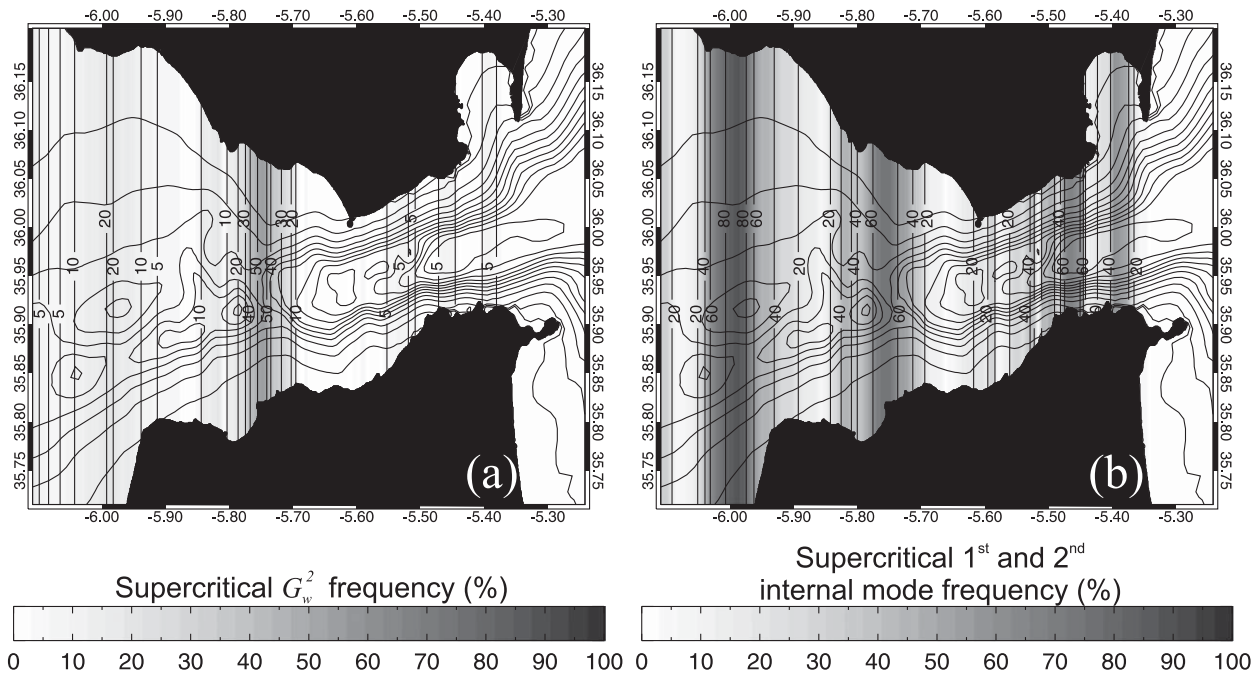
FIG. 11. Frequency of occurrence of supercritical flow for the (a) two-layer and (b) three-layer approximation.

descending tidal phase at Tarifa, and then the control is lost during low water in Tarifa and recovered again during the subsequent rising tidal phase. Due to the diurnal inequality, the flow is supercritical during neap tide only one time per day, while the supercritical condition disappears completely during neap days 27 and 28. A similar general behavior has been found also along TN: the flow is supercritical during the descending tidal phase at Tarifa for every semidiurnal tidal period around spring days, while the duration of supercritical conditions is reduced for every diurnal tidal period

during neap days, disappearing completely during neap days from 26 to 31.

What emerges from the previous description is the absence of any permanent supercritical region along the strait; however, this seems to be in contrast with the simulated character of the flow. For example, in the region of ES the Mediterranean water is always directed westward and subject to a permanent hydraulic jump west of ES. This is confirmed by the abrupt deepening of the isohalines west of ES and by the presence of mixing, which is evidenced by a Richardson number, defined as
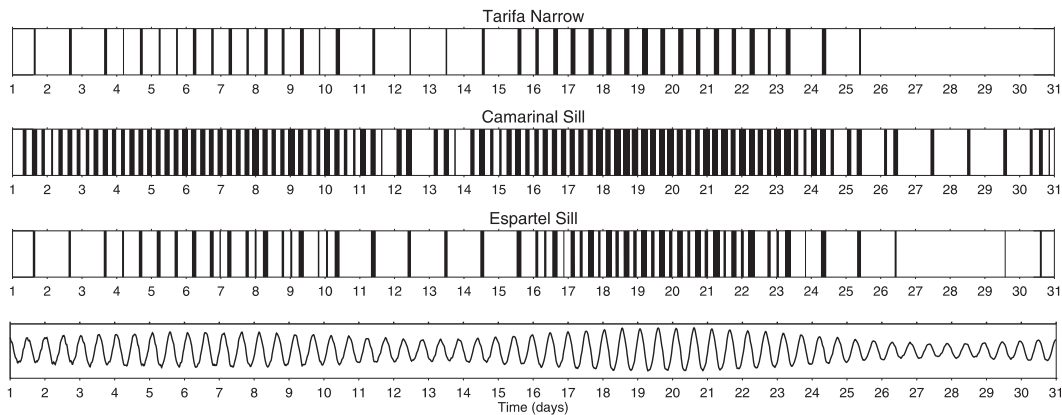

FIG. 12. Bars indicating the presence of supercritical condition, for the two-layer case, in the three main regions of the Strait: ES, CS, and TN. For ES and CS the critical condition is referred to the lower layer, while for TN it is referred to the upper layer. (bottom) Tidal elevation at Tarifa.
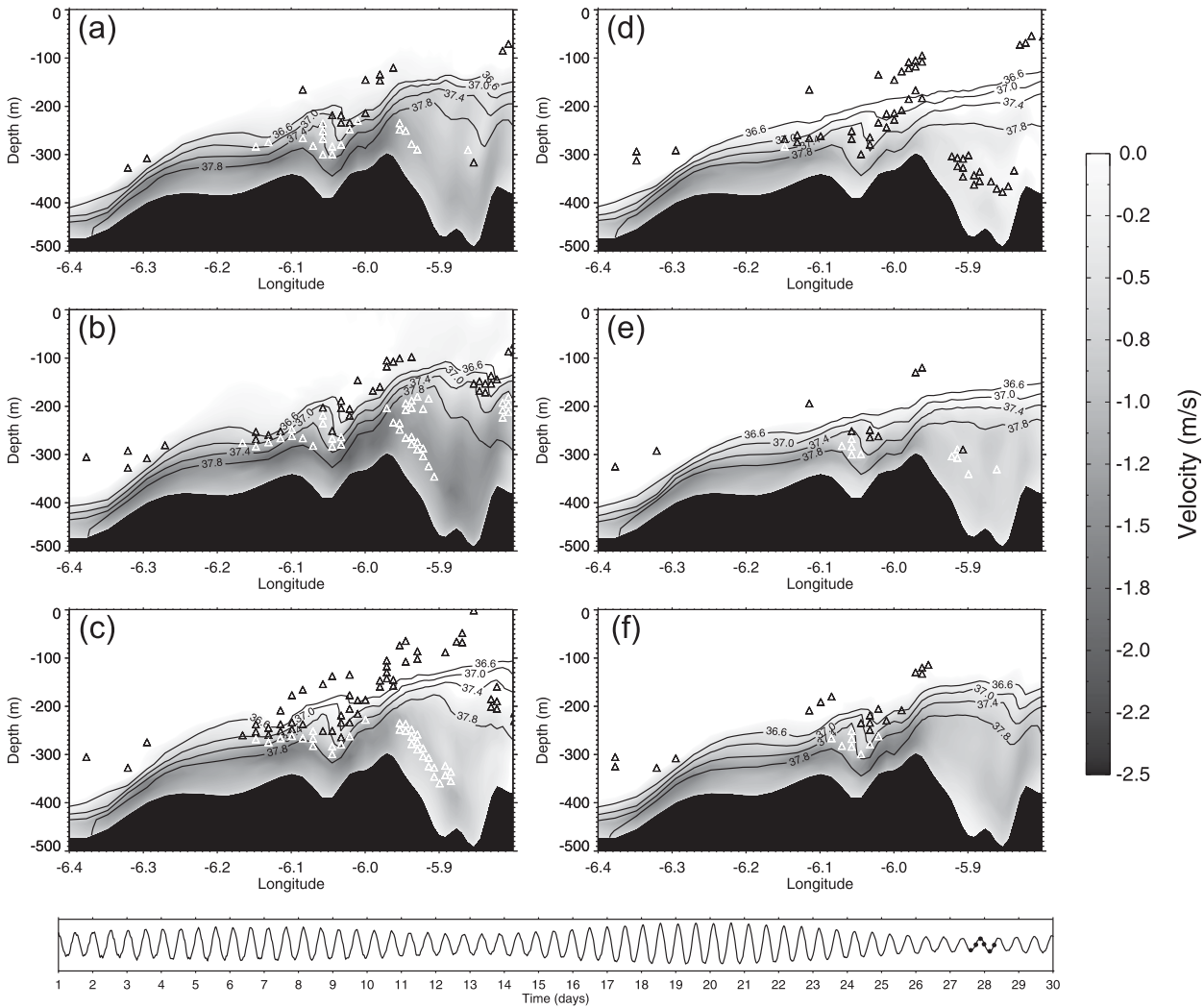
FIG. 13. (a)–(f) Velocity fields along section E during neap tide. Triangles (both black and white) mark the position where the flow reaches a Richardson number less than 0.25. (bottom) Times of the individual snapshots marked on the tidal elevation at Tarifa. Contour lines indicate the position of the isohaline.

$$\mathrm{Ri} = -\frac{g}{\rho_0}\frac{\partial \rho}{\partial z}\left(\frac{du}{dz}\right)^{-2}, \qquad (10)$$

which is always less than the critical value of 0.25 west of ES (Fig. 13). Moreover, looking at the salinity distribution along cross section D, one can note that the Atlantic flow is cyclically detached from the north shore east of TN, even when the two-layer hydraulic model predicts a submaximal flow in TN (Fig. 14). As initially suggested by FA88, and subsequently demonstrated both by Bormans et al. (1986) and Timmermans and Pratt (2005), the separation of the flow from the north shore east of TN is the clear indication that the Atlantic flow has reached a supercritical state. Both evidences reinforce the hypothesis initially put forward by Sannino et al. (2002, 2007)

that the direct application of the two-layer hydraulic theory to the Strait of Gibraltar is not obvious.

b. Three-layer definition and properties

For our three-layer framework we follow BR95 and use the upper and lower limit of the halocline as interfaces. However, a different quantitative method for dividing all salinity profiles into Atlantic layer (AL), interfacial layer (IL), and Mediterranean layer (ML) is used. Salinity profiles are fitted with a hyperbolic tangent; in particular, the upper and lower bounds of the interfacial layer are represented by the intersections of the tangent at the inflection point of the hyperbolic tangent with two vertical lines passing respectively through the simulated salinity at the surface and at the deepest
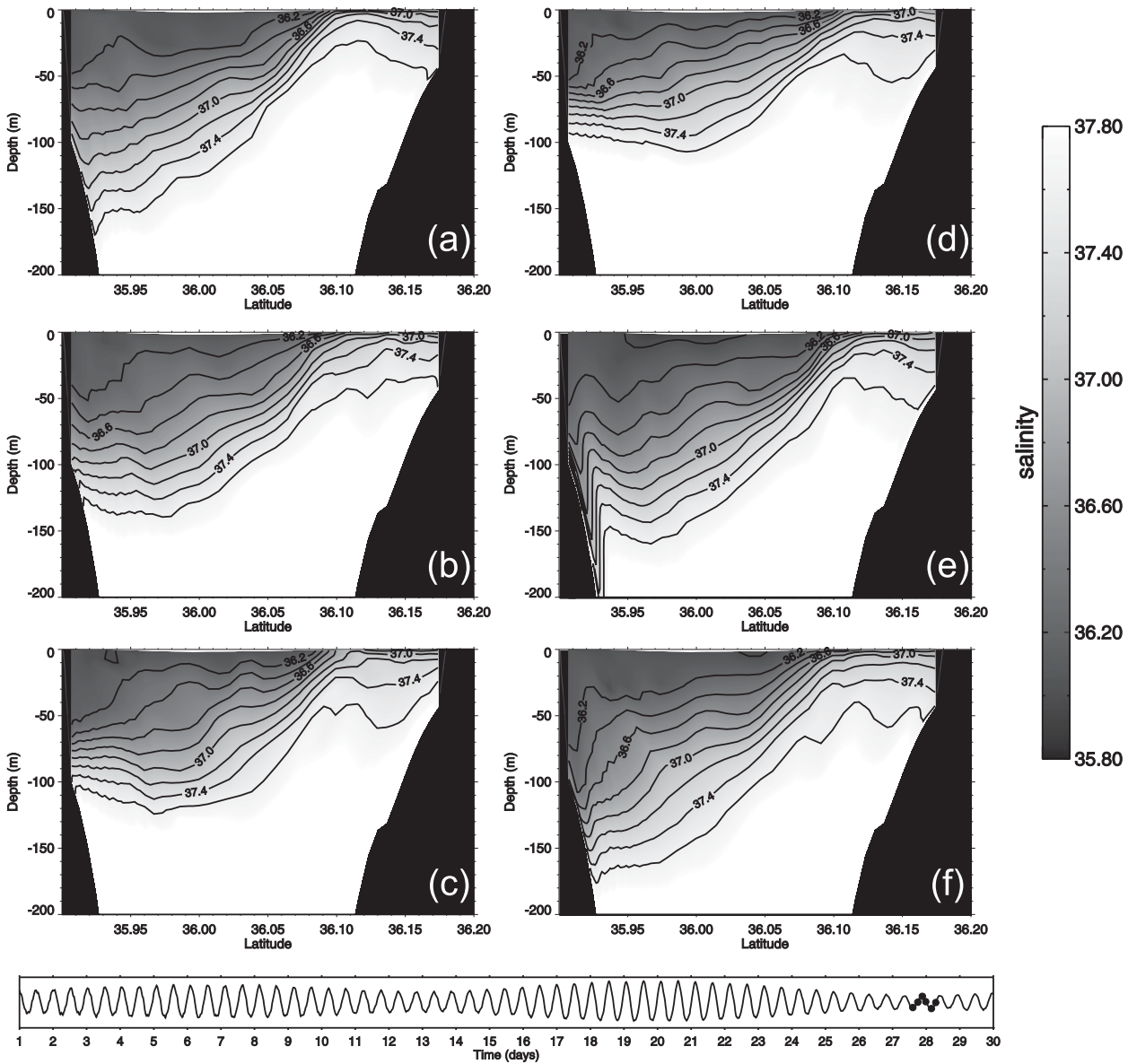
FIG. 14. (a)–(f) Salinity fields along section D during neap tide.

salinity (defined as the arithmetic mean between the deepest simulated salinity and the deepest fitted salinity). To quantitatively measure the fit quality of all salinity profiles, the amount of variance that is explained by the hyperbolic tangent fitting was computed as

$$fq \equiv \left[1 - \left(\sum_k (S_k - \hat{S}_k)^2 \Big/ \sum_k (S_k - \overline{S})^2 \right) \right] \times 100,$$

(11)

where k represents the model vertical levels, S_k is the simulated salinity, $\hat{S}_k$ is the fitted salinity, and $\overline{S}$ is the arithmetic mean of the profiles. Only salinity profiles

with a fit quality $>98\%$ are retained; they however represent more than 90% of the available salinity profiles (about 3500). The mean fit quality value obtained averaging over the entire set of retained salinity profiles is about 99.5%. As an example, three different salinity profiles and the respective fitted curves are shown in Fig. 15.

Figure 16 shows the time-averaged thicknesses of the three layers together with the depth of the midpoint of the interfacial layer. The thickness of AL reduces gradually from west to east except over CS where it undergoes a more evident reduction, halving its value. At the eastern end of TN the effect of rotation becomes
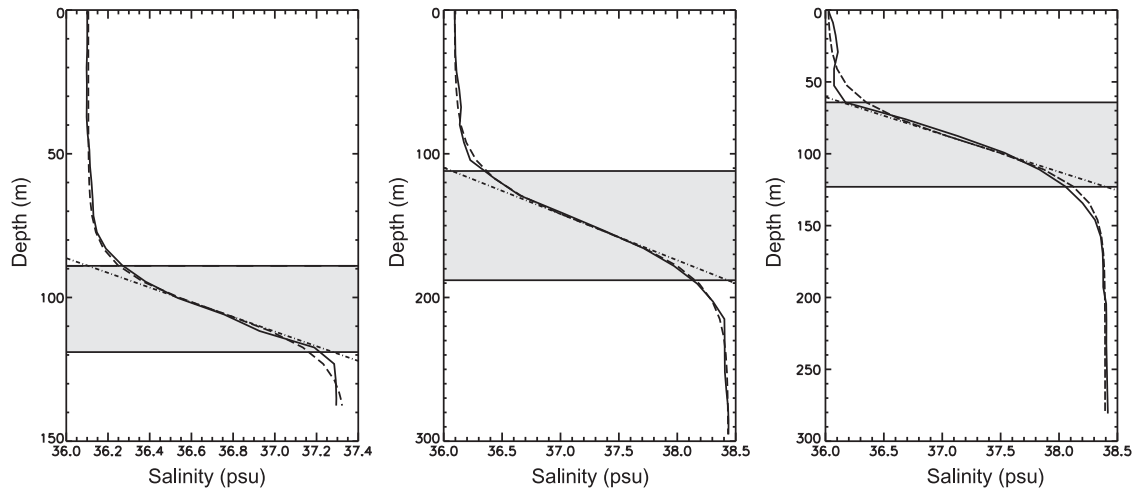
FIG. 15. Comparison between the simulated (solid lines) and the fitted (dashed lines) salinity profiles. The tangent (dashed dotted line) to the flex of the fitted profile and the resulting interfacial layer (gray region) are also plotted.

important and the AL shows a strong cross-strait reduction from the southern to the northern shore. A more dramatic reduction is suffered by ML, which decreases from about 200 to about 50 m over CS. This strong reduction is ascribed to the strong mixing generated by the hydraulic jump that takes place every semidiurnal tidal period west of CS. As pure Mediterranean Water passes over CS, it flows principally along the deep southern channel where it undergoes another mixing due to the hydraulic jump present west of ES. In confirmation of the strong mixing between the two water masses of Atlantic and Mediterranean origin, IL thickness can reach more than 140 m with peaks of about 180 m in the regions where hydraulic jumps are present. The computed midpoint depth of the interfacial layer is in very good agreement with that shown by BR95 (see their Fig. 6); however, the interfacial layer thickness in our case is systematically higher. This difference can be principally attributed to the fact that the analysis of BR95 does not take explicitly into account the tidal variability, while we use simulated data from an entire tropical month tidal period. Another reason is that BR95 analyzed salinity profiles obtained by averaging data collected in November 1985, March 1986, June 1986, and October 1986, while our simulation is performed on a climatological month of April.

Other interesting features can be observed looking at the temporal variability of the interfacial layer thickness that is strongly modulated by tide. Figure 17 shows the interfacial layer thickness as a function of longitude and time. It is referred to section E and covers an entire day during spring and neap tide. Here the presence of the two hydraulic controls west of CS and ES is evident. The interfacial thickness west of ES does not show any sig-

nificant variability, both in space and time, during spring and neap periods. This is, again, a clear indication that the hydraulic jump west of ES is a permanent feature. On the other hand, the interfacial thickness in the region of CS shows a periodic shift of the hydraulic jump from west to east, and vice versa at diurnal frequency. Moreover, the amplitude of the thickness is strongly modulated during the tropical month; in particular, during spring tide it reaches about 200 m on both sides of CS, while during neap tide this value is reached just on the west side, very close to the sill. Finally, the thickness of the interfacial layer at CS shows variability owing to the diurnal inequality of the tide; this is more evident during neap tide.

The instantaneous Atlantic layer transport (ALT), interfacial layer transport (ILT), and Mediterranean layer transport (MLT) for each model cross section within the strait have been computed according to

$$\text{ALT}(x,t) = \int_{y_{S1}(x)}^{y_{N1}(x)} \int_{\text{dw}_1(x,y,t)}^{\text{up}_1(x,y,t)} u(x,y,z,t)\,dz\,dy, \quad (12)$$

$$\text{ILT}(x,t) = \int_{y_{S2}(x)}^{y_{N2}(x)} \int_{\text{dw}_2(x,y,t)}^{\text{up}_2(x,y,t)} u(x,y,z,t)\,dz\,dy, \quad (13)$$

$$\text{MLT}(x,t) = \int_{y_{S3}(x)}^{y_{N3}(x)} \int_{\text{dw}_3(x,y,t)}^{\text{up}_3(x,y,t)} u(x,y,z,t)\,dz\,dy. \quad (14)$$

The resulting transports over the tropical month period are shown in Fig. 18 for four different cross-strait sections located at ES, CS, Tarifa, and Gibraltar, respectively (sections A, B, C, and D in Fig. 8). The Atlantic layer carries water principally toward the east with a
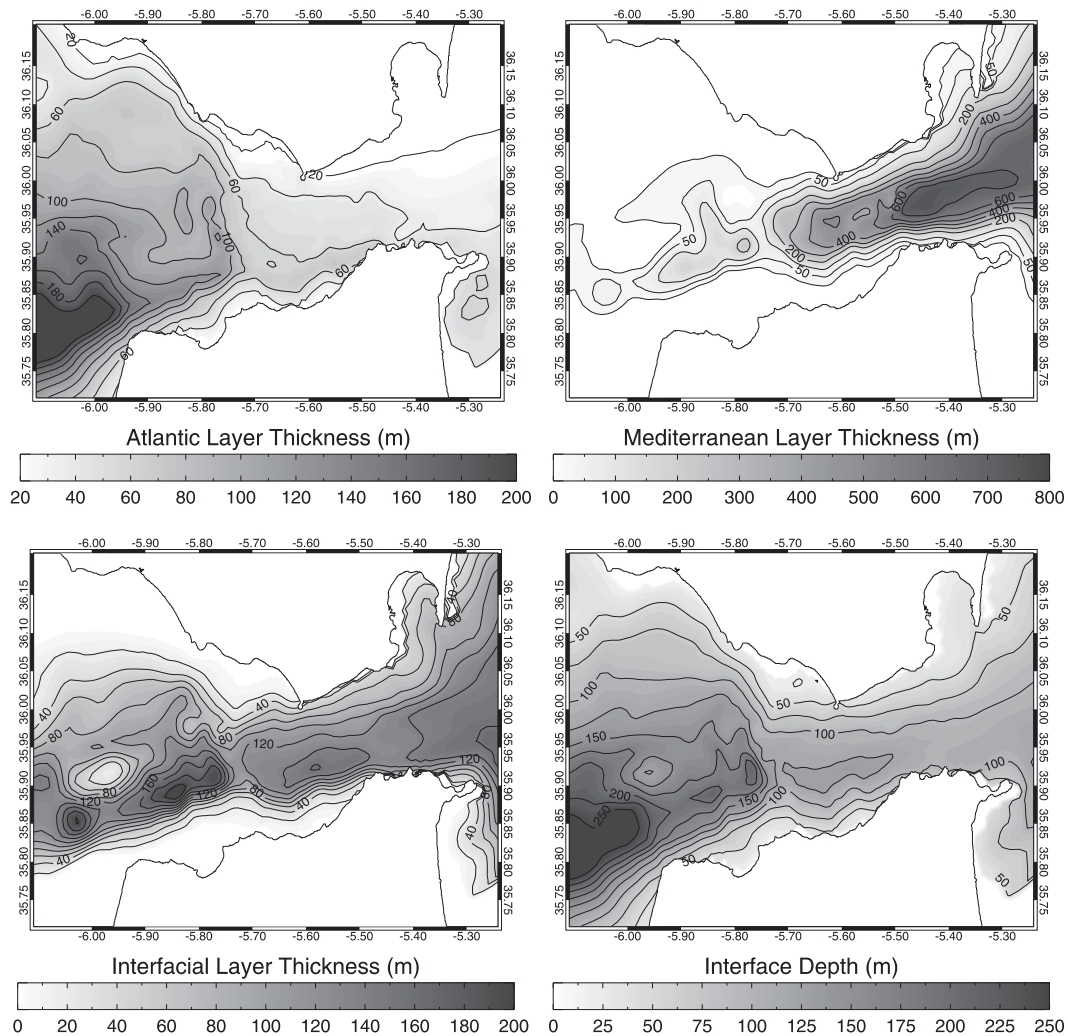
FIG. 16. Time-averaged Atlantic, interfacial, and Mediterranean layer thickness, and depth of the midpoint of the interfacial layer as simulated by the numerical model.

small fraction of the transport cyclically directed also in the opposite direction. This small fraction decreases progressively from west to east becoming null after crossing CS. An opposite behavior is exhibited by MLT where the principal direction is toward the west, and the eastward fraction decreases gradually from section D to section A where it is reduced to zero. Figure 18 also shows that ILT reaches values comparable both with ALT and MLT, contributing to transport-mixed Atlantic–Mediterranean water alternatively in both directions everywhere along the strait. It is noteworthy that the ILT amplitude exceeds the ALT and MLT amplitude at the eastern and western end of the strait, respectively.

c. Three-layer hydraulics

For the three-layer case it is interesting first to ask whether the interfacial layer experiences some interval across the strait over which $(w_3/w_2)\tilde{F}_2^2$ is so small that the upper and lower layers are decoupled. Looking for time intervals in which $(w_3/w_2)\tilde{F}_2^2 \leq 10^{-4}$ over the entire tropical month period, it appears that the upper and lower layers are decoupled only for less than 10% of time everywhere in the strait with minimum values limited to the west of ES, around CS and in the eastern part of TN. Moreover, during these time intervals both upper and lower layer flows are always subcritical. Thus, in order to identify regions where the flow is provisionally supercritical with respect to one or both modes, the instantaneous values of $\tilde{F}_1^2$, $(w_3/w_2)\tilde{F}_2^2$, and $\tilde{F}_3^2$ are computed following (4), and then the rules defined by (6) and (7) are applied. (For simplicity, the terms supercritical and subcritical will hereafter be used instead of provisional supercritical and provisional subcritical.) Results are summarized in Fig. 11b, where the frequency
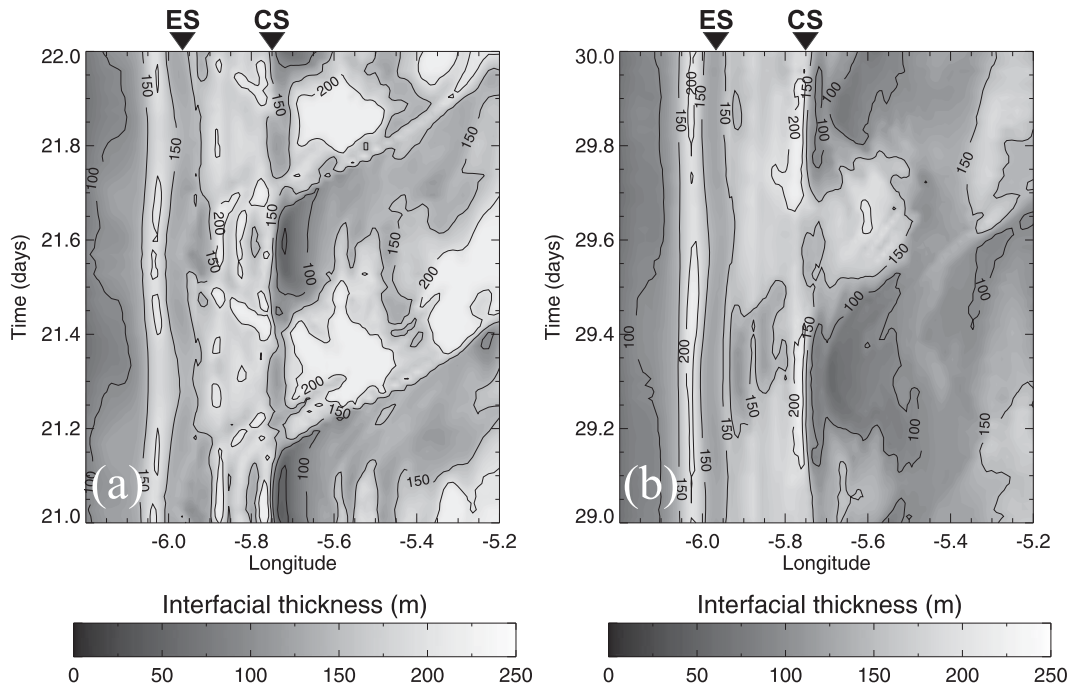
FIG. 17. Interface thickness as a function of longitude and time for the along-strait section E during an entire day corresponding to (a) spring tide and (b) neap tide. The locations of Camarinal Sill and Espartel Sill are marked by a black triangle.

of occurrence over the tropical month period of supercritical flow with respect to at least one mode is shown. Here one can note that supercriticality is reached with higher frequency relative to the two-layer case at ES and TN. In particular, at the eastern end of TN the frequency reaches more than 60%, while west of ES, in accordance with the previous consideration on the flow characteristics, the frequency is about 100%.

Further insight on hydraulics can be gained by looking at the temporal variability of the controlled flow restricted, in the light of the previous findings, to the region of TN and around the two sills of ES and CS (Fig. 19). Black bars in Fig. 19 indicate the presence of supercritical flow due to just one mode, while gray bars mark the instants when the flow is supercritical with respect to both modes. Except around ES where the flow is permanently supercritical, the flow is only intermittently supercritical both in CS and along TN during each diurnal tidal cycle. The frequency of appearance of supercritical flow, with respect to just one mode and with respect to both modes, over the entire tropical month period is about 76% and 67% at TN and CS, respectively. Moreover, while the flow is supercritical with respect to both modes for only 6% in TN, the percentage increases up to 26% at CS. A similar percentage is also found at ES. Thus, while at CS the flow is supercritical with respect to one and both modes with approximately

the same percentage, the flow is principally controlled with respect to only one mode both at ES and TN.

The control along TN always starts to develop at its eastern boundary when the tide is high at Tarifa. During the subsequent descending phase the control extends more and more toward the west along TN, reaching maximum extension after about 4 h. In the remaining descending phase, and also during the subsequent rising phase, that is, when the magnitude of the velocity in the Atlantic layer decreases, the control is progressively lost along TN starting from its western boundary. During spring periods, that is, from day 3 to 8 and from day 16 to 22, the control is completely lost 3 h after low tide, while for the remaining days the control holds until high tide is reached in Tarifa. This different behavior is related to the minimum velocity reached in the upper layer during each semidiurnal tidal cycle. It is known that the upper layer, in the region of TN, is always directed toward the Mediterranean Sea. This is due to the weakness of the tidal amplitude relative to the strong mean current at Tarifa. However, the tide is still able to reduce the magnitude of the upper-layer flow enough to establish subcritical conditions. This reduction is more evident during spring tide than during neap tide and, thus, explains why the control is lost during spring tide and not during neap tide.

At CS the model reproduces the tidally induced periodic loss and subsequent renewal of the control that
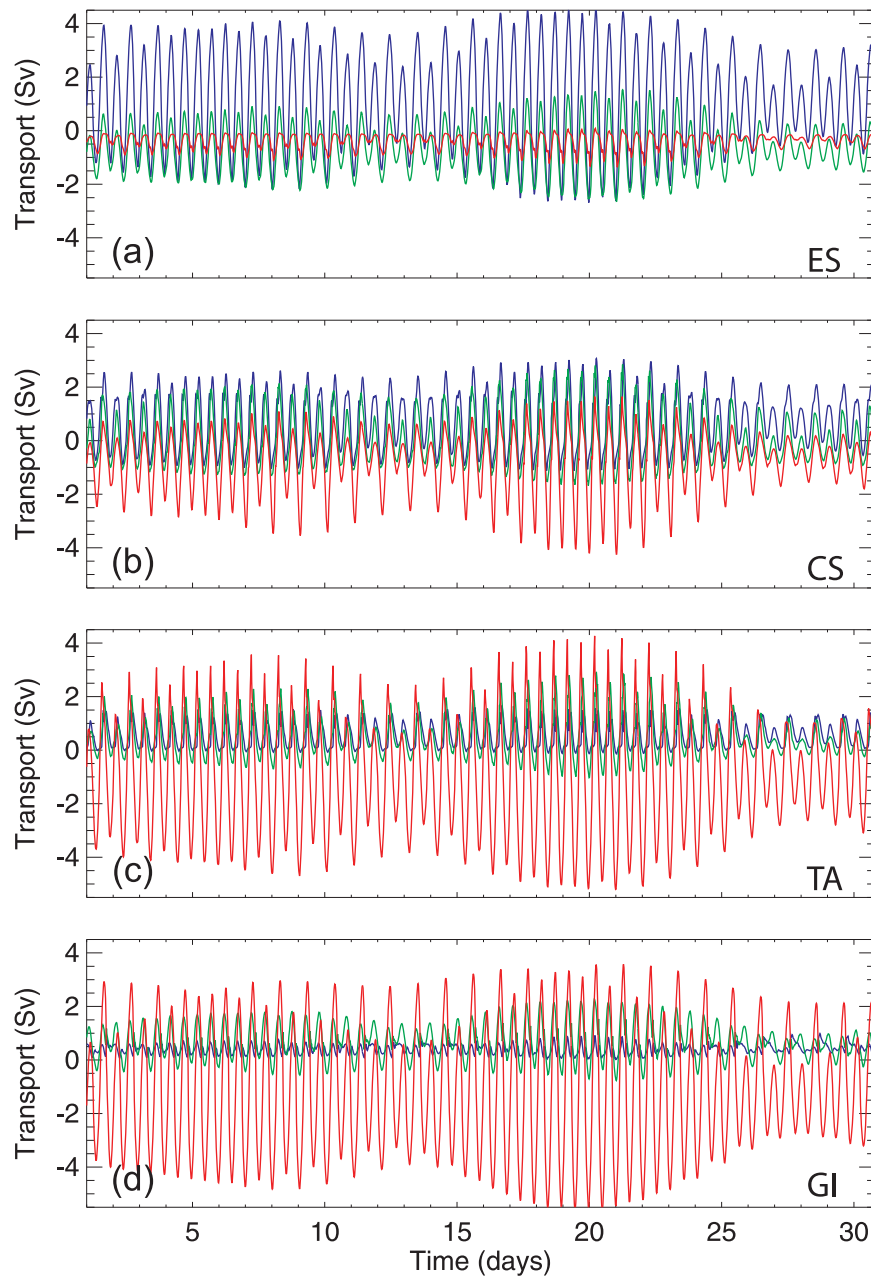
Fig. 18. Time-dependent Atlantic layer (blue line), interfacial layer (green line), and Mediterranean layer (red line) volume transports at (a) Espartel Sill, (b) Camarinal Sill, (c) Tarifa (TA), and (d) Gibraltar (GI), respectively, Figs. 8a–d.

occurs two times for each semidiurnal cycle for the entire period except during neap tide (from day 26 to 29). During rising water at Tarifa the control at Camarinal starts to develop while, during the subsequent descending phase, the control is initially lost, then recovered and lost again during low tide.

From the above description it appears that the exchange switches cyclically between a maximal and submaximal regime, with a permanent control at ES and an intermittent control along TN. In such a configuration CS is not the principal control of the flow at the western end of the strait.

5. Summary and concluding remarks

We have investigated the hydraulic behavior of the exchange flow through the Strait of Gibraltar using the recent hydraulic criterion developed by Pratt (2008).
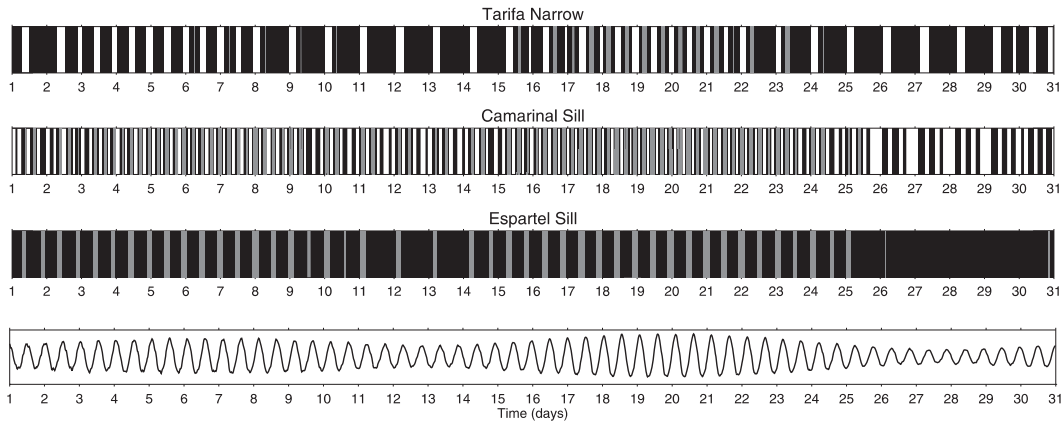
FIG. 19. Bars indicating the presence of provisional supercritical flow with respect to one mode (black) and with respect to both modes (gray) in the three main regions of the strait: Espartel Sill, Camarinal Sill, and Tarifa Narrow. (bottom) Tidal elevation at Tarifa.

The continuous vertical stratification has been approximated first by a two-layer system and then by a three-layer system and cross-strait variations in velocity and layer thickness are accounted for. In the two-layer case the interface has been chosen approximately in the middle of the layer in which entrainment and mixing occur between Mediterranean and Atlantic waters, while for the three-layer case this transition zone has represented one of the three layers. We have focused our attention on the differences induced by the two different vertical approximations on the predicted hydraulic regime in the strait. A three-dimensional numerical simulation reproducing the two-way exchange in the strait at high resolution and tidal frequency has provided data for the hydraulic analysis; in particular, the simulation covered an entire tropical month period.

The hydraulic behavior analyzed in the two-layer framework has predicted intermittent controls at CS, ES, and TN, with a frequency of occurrence of 50%, 23%, and 15% respectively, lower than indicated by previous studies. Comparisons must be made with caution, for previous studies are based on the *local* composite Froude number, often measured near the channel centerline. In reality, G^2 can vary strongly across the channel (Fig. 20), sometimes ranging above and below unity across the same section. Its value at any particular location is not an indicator of hydraulic control. In the TN G^2 remains <1 in the channel center at all times, occasionally exceeding unity along the sides where the shoaling depth causes the layer thickness to decrease. A simple inspection of Fig. 20 does not determine whether the flow at TN is hydraulically subcritical or supercritical; only evaluation of the cross-strait integral condition (2) can decide that question.

Comparisons with previous work must also take into consideration differing definitions of the two-layer in-

terface. For example, FA88 found a permanent hydraulic control at TN, a conclusion that is in disagreement with Fig. 20 showing values of G^2 permanently <1 in the channel center at TN. As an interface at the eastern end of the strait, FA88 used the surface $\sigma_\theta = 28.0$, which corresponds approximately to a salinity of 37.4 psu, and as velocities the values at middepth of each layer. The choice of $\sigma_\theta = 28.0$ is problematic for the eastern part of the strait because it determines an upper layer that is too thin, giving rise to a general overestimation of the upper-layer velocity and overestimation of G^2.
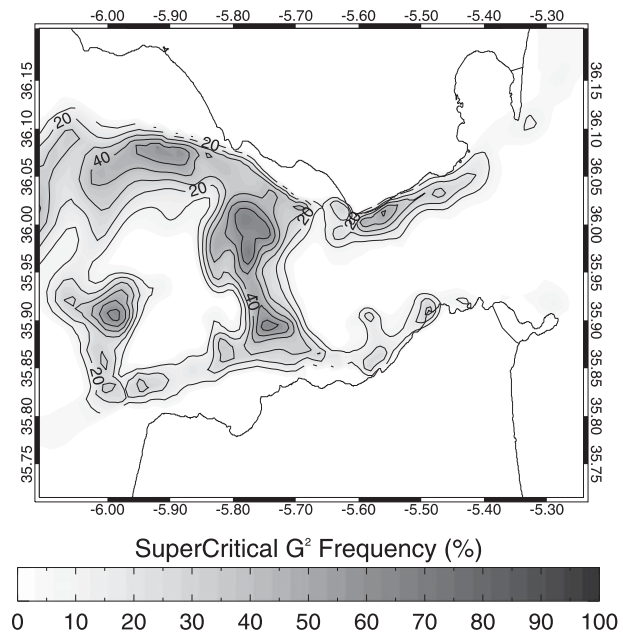

SuperCritical G² Frequency (%)

FIG. 20. Maps of the frequency of occurrence of supercritical local composite Froude numbers for the two-layer one-dimensional case.

That the choice of the interface between the two layers may alter the values of G^2 was already argued by Send and Baschek (2001). They computed the Froude number at the eastern end of the strait, using both the 37.4 and the 38.1 isohaline, as the interface during a complete M_2 tidal cycle for both spring and neap tide during April 1996. For both computations the velocities of the two layers were determined by taking the mean value away from the main shear zone. The results showed that using the 37.4 isohaline as the interface led the flow to appear controlled during part of the tidal cycle, both during neap and spring tide, while using the 38.1 isohaline caused the flow to always appear subcritical. The ambiguity in the computation of the Froude numbers is therefore due in part to the difficulty of fitting a two-layer model to a flow with a substantial interfacial layer. In some cases, investigators are content to estimate the Froude number of the upper (or lower) layer above. This approach corresponds to the implicit assumption that the transition layer is stagnant, implying that the Atlantic layer and the Mediterranean layer are decoupled. However, this is not the case in the Strait of Gibraltar where, as we have demonstrated in section 2, the upper and lower layer are decoupled for only 10% of the total tropical month period and, moreover, during these periods neither of the layers appear to be supercritical at TN.

The analysis carried out by means of the three-layer, two-dimensional hydraulic model has shown substantial differences with respect to the two-layer, two-dimensional model. In the three-layer case the frequency of occurrence of the intermittent controls, both at CS and TN, is increased up to 67% and 76%, respectively, but, more importantly, on the west side of ES the three-layer model predicts a permanent supercritical flow. The character of the simulated exchange flow supports this hydraulic behavior: west of ES the model indicates the presence of a permanent hydraulic jump for the Mediterranean Outflow; along the northern shore of TN there is an intermittent detachment of the upper layer.

The hydraulic analysis also indicates that the exchange flow in the strait switches cyclically between a maximal and submaximal regime during the tropical month period. The maximal regime is achieved when the flow reaches a supercritical condition along TN since the flow at the western end of the strait is nearly always supercritical west of ES. Thus, the simulated flow resulted in a maximal regime two times per day during spring tides, and one time per day during neap tide, for a total of about 76% of the entire tropical month period. It appears that CS plays only a secondary role with respect to ES.

In summary, there are a number of discrepancies between our results and previous results for a two-layer idealization of the Strait of Gibraltar stratification. Our results generally suggest that control acts less often, and at fewer locations. As our numerical simulations appear to match available observations, the discrepancies with previous work are thought to be due to the previous neglect of cross-channel variations in the velocity and layer depth and, more importantly, the ambiguities in fitting a two-layer model to a system with a substantial intermediate layer. Moreover, when we fit our continuously stratified model results to a three-layer system with an active intermediate layer, the results of the hydraulic analysis become more consistent with conventional wisdom about the exchange flow (i.e., that it is predominantly maximal) and with the qualitative behavior of the model itself.

For a more complete understanding of the hydraulic criticality of the exchange flow in the Strait of Gibraltar, one must also account for the meteorological subinertial forcing together with the seasonal long-term forcing. Moreover, the interpretation of maximal and submaximal hydraulic control has been discussed by past authors mainly in the context of two-layer systems that allow no mass exchange between the layers. The Strait of Gibraltar situation, with a third layer and with mass exchange between layers, is more problematic. In labeling the exchange ''maximal'' we have applied the two-layer criterion that two regions of supercritical flow, both carrying information outward (away from the strait), exist. In a three-layer system, one of those regions may be supercritical with respect to a first baroclinic mode and the other with respect to a second baroclinic mode. This situation raises questions of interpretation that would require a formal hydraulic theory for three-layer model that allows for mass exchange between layers. Such a model would be quite ambitious and is beyond the scope of the present work.

REFERENCES

Ambar, I., N. Serra, M. J. Brogueira, G. Cabeciadas, F. Abrantes, P. Freitas, C. Goncialves, and N. Gonzalez, 2002: Physical, chemical and sedimentological aspects of the Mediterranean outflow off Iberia. *Deep-Sea Res. II,* **49,** 4163–4177.

Armi, L., 1986: The hydraulics of two flowing layers with different densities. *J. Fluid Mech.,* **163,** 27–58.

——, and D. M. Farmer, 1988: The flow of Atlantic water through the Strait of Gibraltar. *Prog. Oceanogr.,* **21,** 1–105.

Baines, P., 1995: *Topographic Effects in Stratified Flows*. Cambridge University Press, 482 pp.

Baringer, M. O., and J. F. Price, 1997: Mixing and spreading of the Mediterranean outflow. *J. Phys. Oceanogr.,* **27,** 1654–1677.

Baschek, B., U. Send, J. García-Lafuente, and J. Candela, 2001: Transport estimates in the Strait of Gibraltar with a tidal inverse model. *J. Geophys. Res.,* **106** (C12), 31 033–31 044.

Bills, P., and J. Noye, 1987: An investigation of open boundary conditions for tidal models of shallow seas. *Numerical Modelling: Applications to Marine Systems,* J. Noye, Ed., Elsevier, 159–194.

Blumberg, A. F., and G. L. Mellor, 1987: A description of a three-dimensional coastal ocean circulation model. *Three-Dimensional Coastal Ocean Models,* N. S. Heaps, Ed., Amer. Geophys. Union, 1–16.

Bormans, M., C. Garrett, and K. Thompson, 1986: Seasonal variability of the surface inflow through the Strait of Gibraltar. *Oceanol. Acta,* **9,** 403–414.

Brandt, P., W. Alpers, and J. O. Backhaus, 1996: Study of the generation and propagation of internal waves in the Strait of Gibraltar using a numerical model and synthetic aperture radar images of the European ERS1 satellite. *J. Geophys. Res.,* **101** (C6), 14 237–14 252.

Bray, N. A., J. Ochoa, and T. H. Kinder, 1995: The role of the interface in exchange through the Strait of Gibraltar. *J. Geophys. Res.,* **100** (C6), 10 755–10 776.

Bryden, H., and H. Stommel, 1984: Limiting processes that determine basic features of the circulation in the Mediterranean Sea. *Oceanol. Acta,* **7,** 289–296.

——, and T. Kinder, 1991: Steady two-layer exchange through the Strait of Gibraltar. *Deep-Sea Res.,* **38** (Suppl.), S445–S463.

——, J. Candela, and T. Kinder, 1994: Exchange through the Strait of Gibraltar. *Prog. Oceanogr.,* **33,** 201–248.

Candela, J., C. D. Winant, and H. L. Bryden, 1989: Meteorologically forced subinertial flows through the Strait of Gibraltar. *J. Geophys. Res.,* **94** (C9), 12 667–12 679.

——, ——, and A. Ruiz, 1990: Tides in the Strait of Gibraltar. *J. Geophys. Res.,* **95,** 7313–7335.

Egbert, G., and L. Erofeeva, 2002: Efficient inverse modeling of barotropic ocean tides. *J. Atmos. Oceanic Technol.,* **19,** 183–204.

Ezer, T., 2005: Entrainment, diapycnal mixing and transport in three-dimensional bottom gravity current simulations using the Mellor–Yamada turbulence scheme. *Ocean Modell.,* **9,** 151–168.

Farmer, D. M., and L. Armi, 1988: The flow of Mediterranean water through the Strait of Gibraltar. *Prog. Oceanogr.,* **21,** 1–105.

Foreman, M. G. G., 1978: Manual for tidal currents analysis and prediction. Institute of Ocean Sciences, Patricia Bay, Pacific Marine Science Rep. 78–6, 57 pp.

García-Lafuente, J., 1986: Variabilidad del nivel del mar en el Estrecho de Gibraltar: Mareas y oscilaciones residuales (Sea level variability in the Strait of Gibraltar: Tides and residual oscillations). Ph.D. thesis, Instituto Español de Oceanografiá, 154 pp.

——, J. Vargas, F. Plaza, T. Sarhan, J. Candela, and B. Bascheck, 2000: Tide at the eastern section of the Strait of Gibraltar. *J. Geophys. Res.,* **105** (C6), 14 197–14 213.

Garrett, C., M. Bormans, and K. Thompson, 1990: Is the exchange through the Strait of Gibraltar maximal or submaximal? *The Physical Oceanography of Sea Straits,* L. Pratt, Ed., Kluwer Academic, 217–294.

Haney, R. L., 1991: On the pressure gradient force over steep topography in sigma coordinate ocean models. *J. Phys. Oceanogr.,* **21,** 610–619.

Izquierdo, A., L. Tejedor, D. V. Sein, J. O. Backhaus, P. Brandt, A. Rubino, and B. A. Kagan, 2001: Control variability and internal bore evolution in the Strait of Gibraltar: A 2-d two-layer model study. *Estuarine Coastal Shelf Sci.,* **53,** 637–651.

Kinder, T., and H. Bryden, 1987: 1985–1986 Gibraltar experiment: Data collection and preliminary results. *Eos, Trans. Amer. Geophys. Union,* **68,** 786–795.

MEDAR Group, 2002: *Medatlas/2002 Database: Mediterranean and Black Sea Database of Temperature, Salinity and Bio-chemical Parameters.* IFREMER Climatological Atlas, CD-ROM.

Mellor, G., and T. Yamada, 1982: Development of a turbulence closure model for geophysical fluid problems. *Rev. Geophys. Space Phys.,* **20,** 851–875.

——, T. Ezer, and L. Oey, 1994: The pressure gradient conundrum of sigma coordinate ocean models. *J. Atmos. Oceanic Technol.,* **11,** 1126–1134.

Orlanski, I., 1976: A simple boundary condition for unbounded hyperbolic flows. *J. Comput. Phys.,* **21,** 251–269.

Pawlowicz, R., B. Beardsley, and S. Lentz, 2002: Classical tidal harmonic analysis including error estimates in MATLAB using T_Tide. *Comput. Geosci.,* **28,** 929–937.

Pratt, L., 2008: Critical conditions and composite Froude numbers for layered flow with transverse variations in velocity. *J. Fluid Mech.,* **602,** 241–266.

——, W. Johns, S. P. Murray, and K. Katsumata, 1999: Hydraulic interpretation of direct velocity measurements in the Bab al Mandab. *J. Phys. Oceanogr.,* **29,** 2769–2784.

Reid, J. L., 1979: On the contribution of the Mediterranean Sea outflow to the Norwegian–Greenland Sea. *Deep-Sea Res. I,* **26,** 1199–1223.

Sanchez-Roman, A., G. Sannino, J. Garcia-Lafuente, A. Carillo, and F. Criado-Aldeanueva, 2009: Transport estimates at the western section of the Strait of Gibraltar: A combined experimental and numerical study. *J. Geophys. Res.,* **114,** C06002, doi:10.1029/2008JC005023.

Sannino, G., A. Bargagli, and V. Artale, 2002: Numerical modeling of the mean exchange through the Strait of Gibraltar. *J. Geophys. Res.,* **107,** 3094, doi:10.1029/2001JC000929.

——, A. Carillo, and V. Artale, 2007: Three-layer view of transports and hydraulics in the Strait of Gibraltar: A three-dimensional model study. *J. Geophys. Res.,* **112,** C03010, doi:10.1029/2006JC003717.

Send, U., and B. Baschek, 2001: Intensive shipboard observations of the flow through the Strait of Gibraltar. *J. Geophys. Res.,* **106** (C12), 31 017–31 032.

Smeed, D., 2000: Hydraulic control of three-layer exchange flows: Application to the Bab al Mandab. *J. Phys. Oceanogr.,* **30,** 2574–2588.

Smolarkiewicz, P., 1984: A fully multidimensional positive definite advection transport algorithm with small implicit diffusion. *J. Comput. Phys.,* **54,** 325–362.

Stommel, H., and H. Farmer, 1953: Control of salinity in an estuary by a transition. *J. Mar. Res.,* **12,** 13–20.

Timmermans, M. E., and L. J. Pratt, 2005: Two-layer rotating exchange flow between two deep basins: Theory and application to the Strait of Gibraltar. *J. Phys. Oceanogr.,* **35,** 1568–1592.

Tsimplis, M., R. Proctor, and R. Flather, 1995: A two-dimensional tidal model for the Mediterranean Sea. *J. Geophys. Res.,* **100** (C8), 16 223–16 239.

U.S. Department of Commerce and NOAA/NGDC, 2001: (ETOPO2) 2-minute gridded global relief data. Digital media. [Available online at http://www.ngdc.noaa.gov.]

Wesson, J., and M. Gregg, 1994: Mixing at Camarinal sill in the Strait of Gibraltar. *J. Geophys. Res.,* **99** (C5), 9847–9878.